THE CRYSTALLIZATION OF K-FELDSPAR MEGACRYSTS IN GRANITOIDS FROM SOUTHWESTERN NOVA SCOTIA

Derek Wongus

Submitted in Partial Fulfilment of the Requirements
for the Degree of Bachelor of Sciences, Honours
Department of Earth Sciences
Dalhousie University, Halifax, Nova Scotia
March 2013

Distribution License

DalSpace requires agreement to this non-exclusive distribution license before your item can appear on DalSpace.

NON-EXCLUSIVE DISTRIBUTION LICENSE

You (the author(s) or copyright owner) grant to Dalhousie University the non-exclusive right to reproduce and distribute your submission worldwide in any medium.

You agree that Dalhousie University may, without changing the content, reformat the submission for the purpose of preservation.

You also agree that Dalhousie University may keep more than one copy of this submission for purposes of security, back-up and preservation.

You agree that the submission is your original work, and that you have the right to grant the rights contained in this license. You also agree that your submission does not, to the best of your knowledge, infringe upon anyone's copyright.

If the submission contains material for which you do not hold copyright, you agree that you have obtained the unrestricted permission of the copyright owner to grant Dalhousie University the rights required by this license, and that such third-party owned material is clearly identified and acknowledged within the text or content of the submission.

If the submission is based upon work that has been sponsored or supported by an agency or organization other than Dalhousie University, you assert that you have fulfilled any right of review or other obligations required by such contract or agreement.

Dalhousie University will clearly identify your name(s) as the author(s) or owner(s) of the submission, and will not make any alteration to the content of the files that you have submitted.

If you have questions regarding this license please contact the repository manager at dalspace@dal.ca.

Grant the distribution license by signing and dating below.

_____ _____

Name of signatory Date

DATE _____

AUTHOR _____

TITLE
_____

_____

_____

Degree _____ Convocation _____ Year _____

Permission is herewith granted to Dalhousie University to circulate and to have copied for non-commercial purposes, at its discretion, the above title upon the request of individuals or institutions.

_____

Signature of Author

Abstract

The magmatic growth of K-feldspar megacrysts from the Halifax Pluton has been investigated. The study consisted of detailed textural characterization of two separate samples of granitic rocks from Peggy's Cove and Prospect, Nova Scotia. The whole-rock textures, megacryst concentrations, and crystal shapes suggest a different magmatic history for these samples. Detailed petrographic studies further suggest different crystallization histories for these two areas. Specifically, the sample from Peggy's Cove shows far fewer megacrysts and also less euhedral grain shapes. The megacrysts are also less strongly zoned and contain fewer large inclusions. The megacrysts from Prospect display oscillatory zoning and abundant, aligned inclusions, including inclusions of oscillatory zoned plagioclase. Barium and other elements define zoning in megacrysts which suggests that magma mixing and resorption of the megacrysts has occurred. This is particularly pronounced in the Peggy's Cove sample. Using two-feldspar (plagioclase and alkali feldspar) geothermometry to determine temperature variability within the megacrysts, the temperatures recorded for the high temperature phase of megacryst growth are 832^{o}C to 913^{o}C in Peggy's Cove and 670^{o}C to 770^{o}C at Prospect. This, along with the textural differences and the chemical zonation in the megacrysts strongly suggests that the sample from Peggy's Cove underwent a period of resorption and regrowth due to an increase in the magma temperature. The most likely explanation for this is a magma mixing event. The relationship between Ba in the megacrysts and the differences in local temperatures recorded in these two samples suggests a difference in the effects of magma mixing and that the increase in temperature caused by this event was focused in the Peggy's Cove area. The temperature ranges recorded by perthite exsolutions are also different. Peggy's Cove records a temperature range of between 483^{o}C and 520^{o}C, with a higher temperature range of 530^{o}C to 586^{o}C being recorded at Prospect. This lends further support to the suggestion that the megacrysts at Peggy's Cove were re-equilibrated and partially resorbed at high temperatures where they also experienced some Ca-loss. On the other hand, the megacrysts at Prospect have not experienced resorption and thus, did not undergo significant Ca-loss. Thus, subsequent perthite exsolution occurred at higher temperatures in the more Ca-rich megacrysts at Prospect and at a lower temperatures in megacrysts from Peggy's Cove which were already lower in Ca. The results confirm the observations from an increasing number of studies which have documented the dynamic and heterogeneous nature of magmatic crystallization mechanisms in granitic rocks.

Table of Contents

Table of Figures

Acknowledgements

I would like to give a special 'thank you' to my supervisors Richard Cox and Anne-Marie Ryan for their mentoring and patience. Without them there would be no project. I would also like to give acknowledgement to Martin Gibling, Isabelle Coutand, Nick Culshaw, Grant Wach, Brant Laidler, and Gordon Brown. Every kind word, words of encouragement, and advice has not been forgotten.

Chapter 1: Introduction

1.1 Opening Statement

This study analyses the nature of granitic potassium feldspar (K-feldspar) megacrysts from the South Mountain Batholith (SMB) to determine if there is evidence of magma mixing (mingling). Magma mixing is a condition of disequilibrium in melts, and occurs when two or more magmas of different chemical and/or physical properties interact, which can create a heterogeneous magmatic environment (Slaby & Gotze, 2004). As suggested by Slaby and Gotze (2004), disequilibrium affects 'nucleation and growth rates'. The granitoid rocks of Peggy's Cove and Prospect, Nova Scotia show some characteristics that suggest heterogeneity. Other general processes that may contribute to heterogeneity include contamination, assimilation, and crystal fractionation (Winter, 2010). Contamination is the process where wall rock detaches from the larger country rock and is incorporated into the magma. The dislodged wall rock can change the composition of the magma by melting some minerals in the country rocks, this process is dependent on ion exchange and the heat provided by the magma, which cools as it contacts the country rocks (Winter, 2010).

1.2 Overview

Evidence for heterogeneity as seen in Peggy's Cove (PC) - Prospect Area (PA) granitoids include: flow structures defined by the orientation of the megacrysts; colour variation on weathered surfaces; and mantled, zoned phenocrysts. All of these features can indicate magma mixing. The mineral, K-spar is shown to crystallize early in magma cooling (Moore & Sisson, 2008). However some research contests a later timing of K-feldspar crystallization as a result of thermal cycling and suggests that the crystallization took place later in the petrologic history

(Johnson &Glazner, 2010). This research focuses on the distribution in barium (Ba) and textural features in plagioclase phenocrysts from the Unzen volcano by Browne et al. (2006), the K-feldspar of the SMB coarse to medium grained granitoids by Clarke & Clarke (1998), the K-feldspar megacrysts of the Shap granite by Cox et al. (1996), and the various K-feldspar megacrysts discussed by Vernon & Paterson (2008).

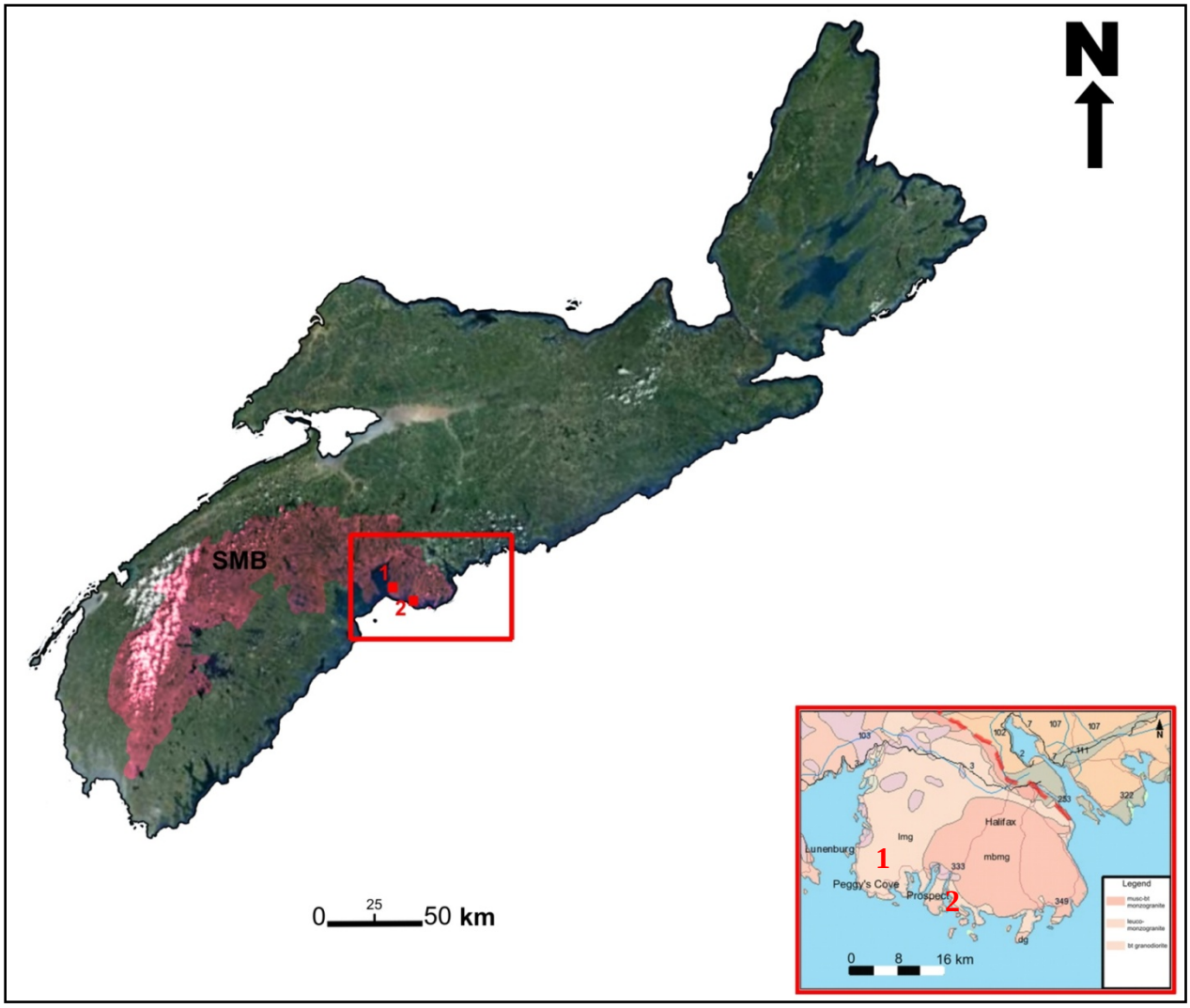

Figure 1.1 A map with county overlay lines of Nova Scotia after Google (2013) and Department of Natural Resources (2013). The South Mountain Batholith (SMB) is indicated by pink hue; the study areas are located in the eastern part of the SMB labelled 1 (Peggy's Cove) and 2 (Prospect).

1.3 Purpose and Objective

The purpose of investigating the crystallization and growth of megacrysts in the Halifax Pluton is to understand the factors that influence the development of heterogeneity in these rocks. The following processes are indicators of magma mixing: nucleation rates, growth stage, and barium concentrations in K-feldspar megacrysts in granitic rocks show an interaction between the crystal and surrounding magma (Browne et al., 2006). These features indicate the time sequence of formation within the crystal, and suggests the confirmation of heterogeneity directly as a result of internal magma processes rather than contamination by country rock. Three objectives will be addressed in this research, which include:

(1) to determine whether Ba and other elements define zoning in megacrysts;

(2) establish whether, on the basis of the nature of the zoning, magma mixing could have occurred;

(3) use of two-feldspar (plagioclase and alkali feldspar) geothermometry to determine temperature variability with the megacrysts.

Chapter 2: Area of Study

2.1 Geological setting

The South Mountain Batholith (SMB), is located in the southwestern part of Nova Scotia. It is a large batholith with an outcrop area of 7300 km², emplaced at 370 Ma, and intruded as part of the Acadian Orogeny, a mountain-building event that included metamorphism, tectonism, and magmatism (MacDonald et al., 1992, 2001). The batholith is a composite intrusion comprised of 13 separate plutons, which can be subdivided into early stage 1 plutons and later stage 2 plutons (MacDonald et al., 1992). Stage 1 plutons are dominated by granodiorite-monzogranite composition. Stage 2 plutons, with intrusive contacts into stage 1 plutons, are dominantly biotite monzogranite-leucomonzogranite in composition. The study area is within a stage 2 biotite monzogranite pluton, within the Peggy's Cove -Prospect area, a component of the Halifax Pluton in southwest N.S.

The granitoid samples for this study are located along the southwest coast of central Nova Scotia and is part of the SMB (Figure 2.1). A distinctive characteristic of the batholith, is its peraluminous nature, suggesting considerable bedrock contamination (MacDonald et al., 1992). In the area of the study, there are biotite monzogranites, which have little to trace amounts of muscovite and are recognized as part of a stage 2 pluton, samples for this research were taken from the biotite monzogranite (MacDonald et al., 1992). The biotite monzogranite is reported to be medium-coarse grained, 10-17% biotite, and have trace amounts of muscovite and cordierite (MacDonald et al., 1992). Other research by MacDonald et al.(1992) identified a number of differences between a stage 1 and 2 pluton including:

(1) stage 2 plutons invariably intrude stage 1 plutons;

(2) one stage 1 and five stage 2 plutons are compositionally unzoned

whereas several stage 1 and 2 plutons display normal and/or reverse zoning;

(3) prominent north-east trending primary flow features (schlieren, parallel alignment of megacrysts/xenoliths) are common in stage 1 plutons whereas they are variably developed (nonexistent to strong) with erratic or concentric orientations in stage 2 plutons.

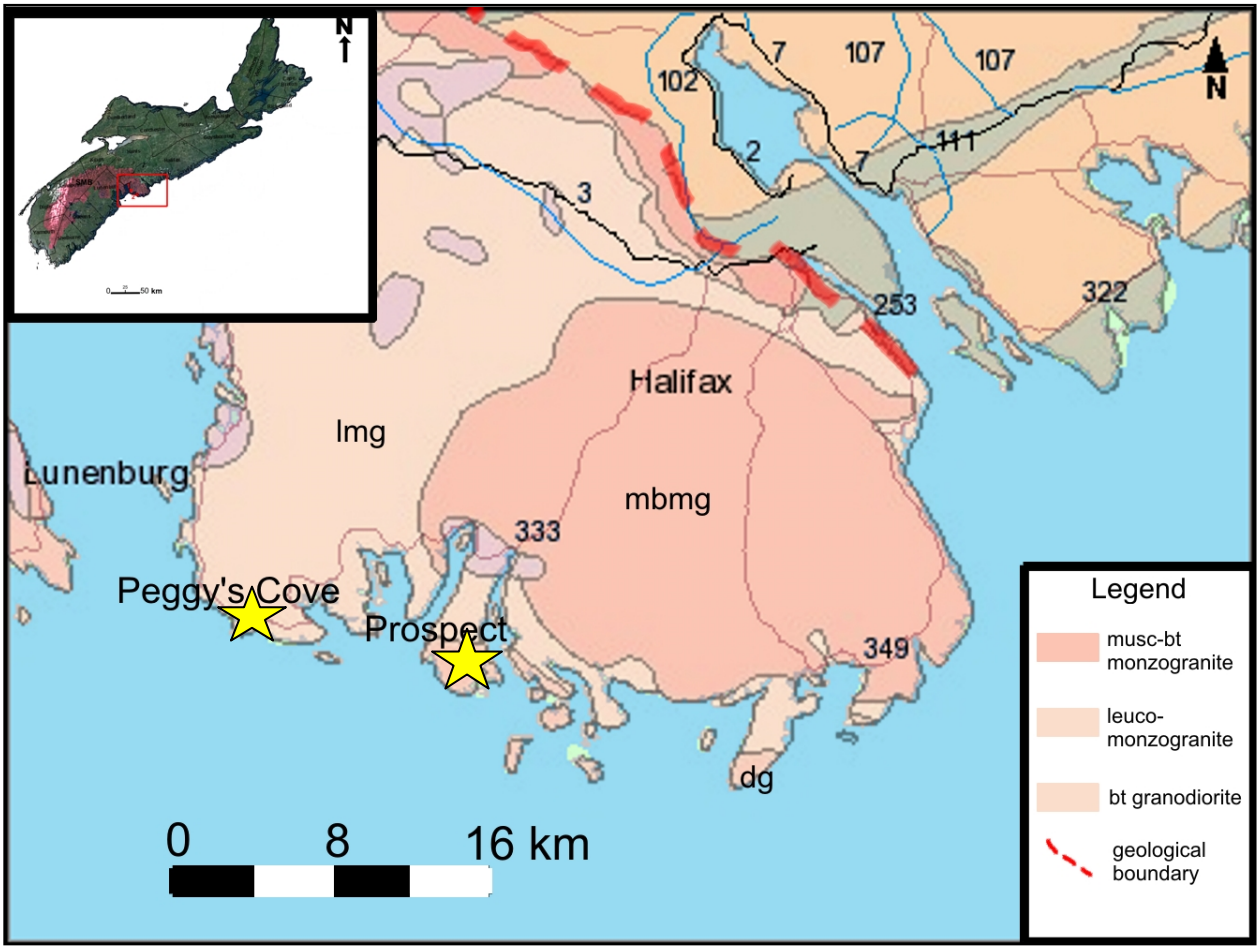

Figure 2.1. A map with a geological overlay of the sample areas in the SMB. The geological segments of the SMB are separated from the Halifax and Goldenville Formations by a broken line marking the boundary.

In this research, there will be some discussion of the features of stage 2 plutons and this information will be used to consider the cooling history of the stage 2 granitoid bodies as evidence by the Halifax Pluton.

Areas of the batholith (Big Indian Lake Pluton, East Dalhousie Pluton and West Dalhousie Pluton) show that there are tectonic controls on the structure (regional faulting), and this is seen in a regional structural geological map (see Fig. 2.2). MacDonald et al. (1992) suggest that stage 2 plutons have occurred on pre-existing structures (Fig. 2.2).

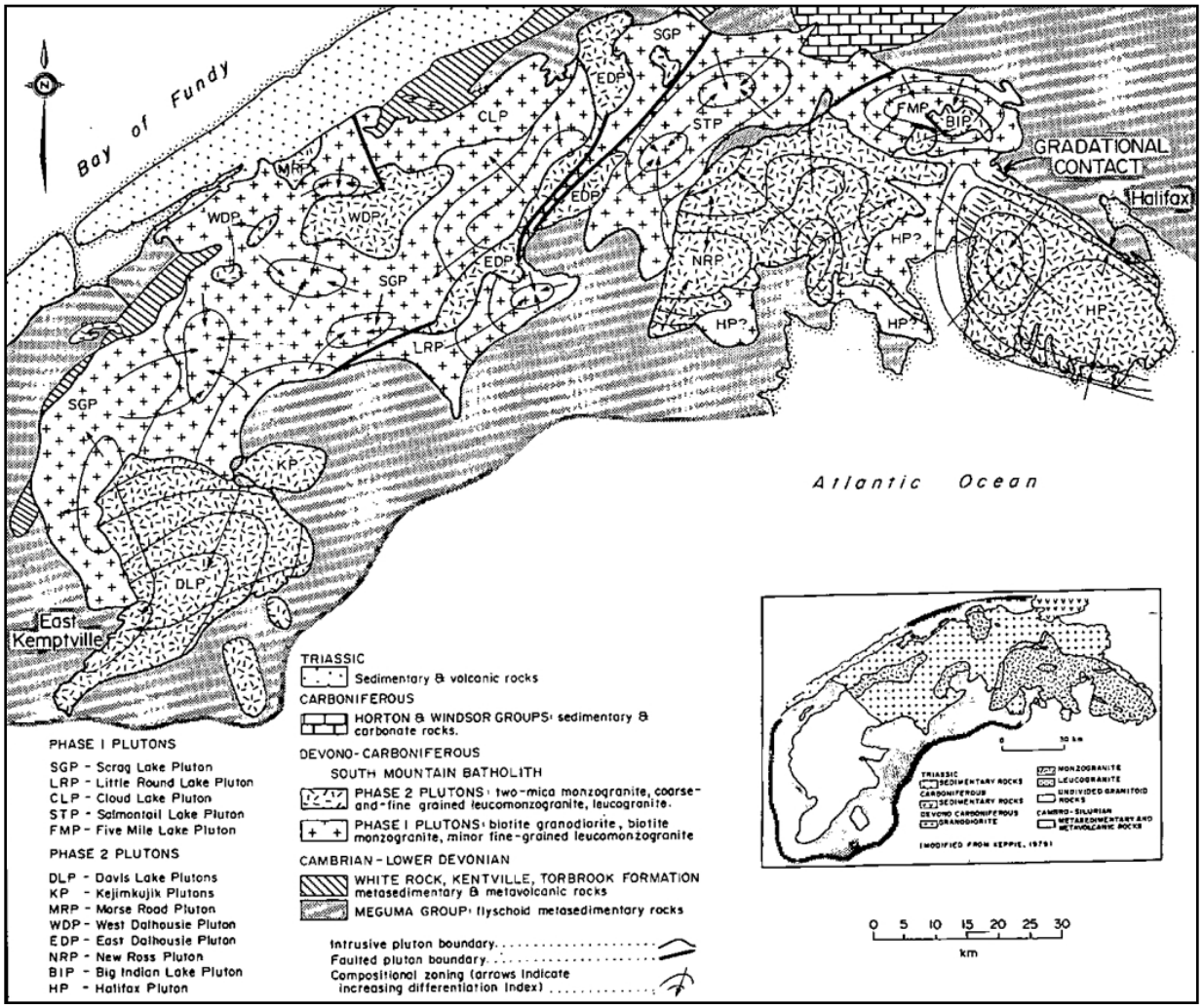

Figure 2.2. A map from MacDonald et al., 1992. The local structural and compositional component of the SMB. Indicated by the box, the Peggy's Cove and Prospect Areas lie within a zoned region of the pluton: the zoning being defined by changes in plagioclase composition and differentiation index (MacDonald et al., 1992).

As indicated in Figure 2.3, the compositional map of Nova Scotia, the area of study has compositional zoning. The zoning shows variation in the differentiation index; the lines that define the compositional gradation are known as isopleths (Fig. 2.3). Compositional zoning is best represented by: (1) changes in anorthite content of plagioclase feldspars; (2) non-uniform K-

feldspar megacrystic compositions; (3) changes in the ratios of K-feldspars to plagioclase; and (4) biotite and quartz proportions (MacDonald et al., 1992). The differentiation index is a quantitative measure of felsic to mafic mineral components found in rocks. In plutonic complexes, the minerals transition to more felsic phases with increasing differentiation. The arrows shown in Figure 2.3 indicate the direction of increase of the differentiation index.

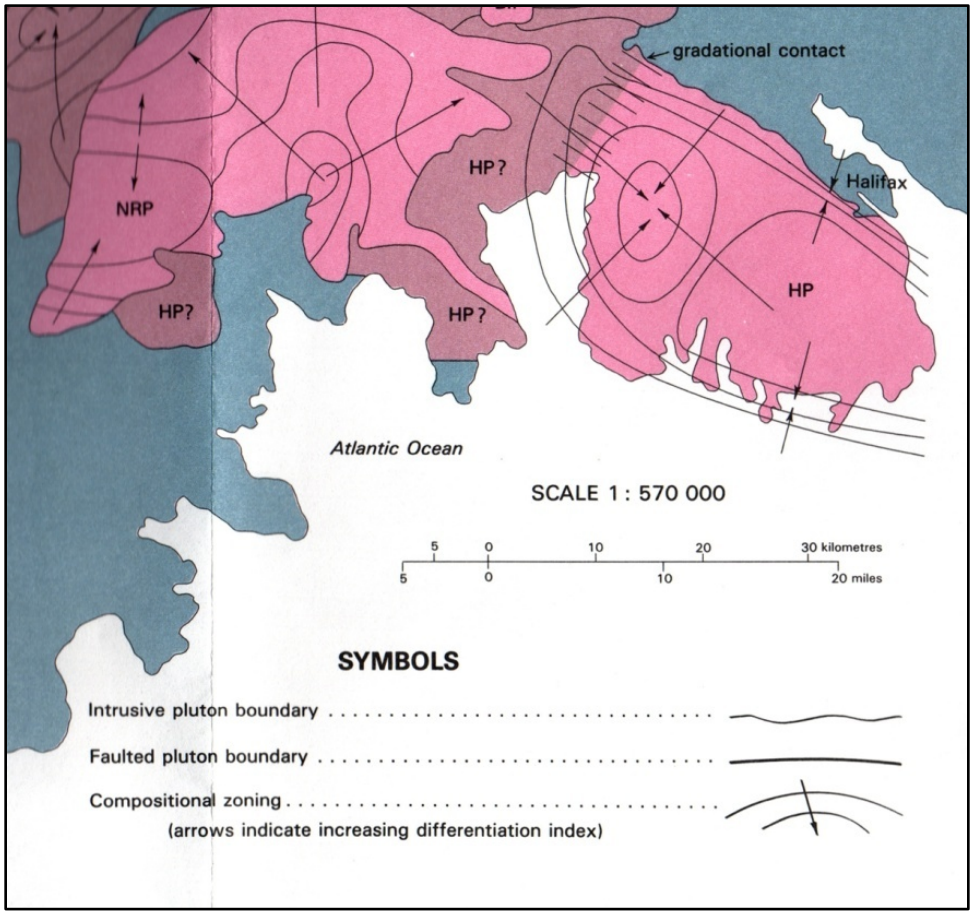

Figure 2.3. A compositional map after Nova Scotia Department of Natural Resources, (1994). The stage 2 type plutons are coloured with pink; whereas, stage 1 plutons are coloured in dark pink. The map shows a stage 1 units that may be the parts of an earlier stage of the Halifax Pluton.

The two sample locations, Peggy's Cove and Prospect came from a less differentiated and more differentiated component respectively. Data gathering for this study focused on microscopy and geochemistry of minerals, and trace elements barium (Ba) and strontium (Sr) in particular, using analysing techniques, similar to research by Cox et al. (1996). Research by Long and Luth

(1986) suggests the Ba concentrations within a K-feldspar megacryst in relation with the diffusion coefficient can indicate the conditions of crystallization (Fig. 2.4).

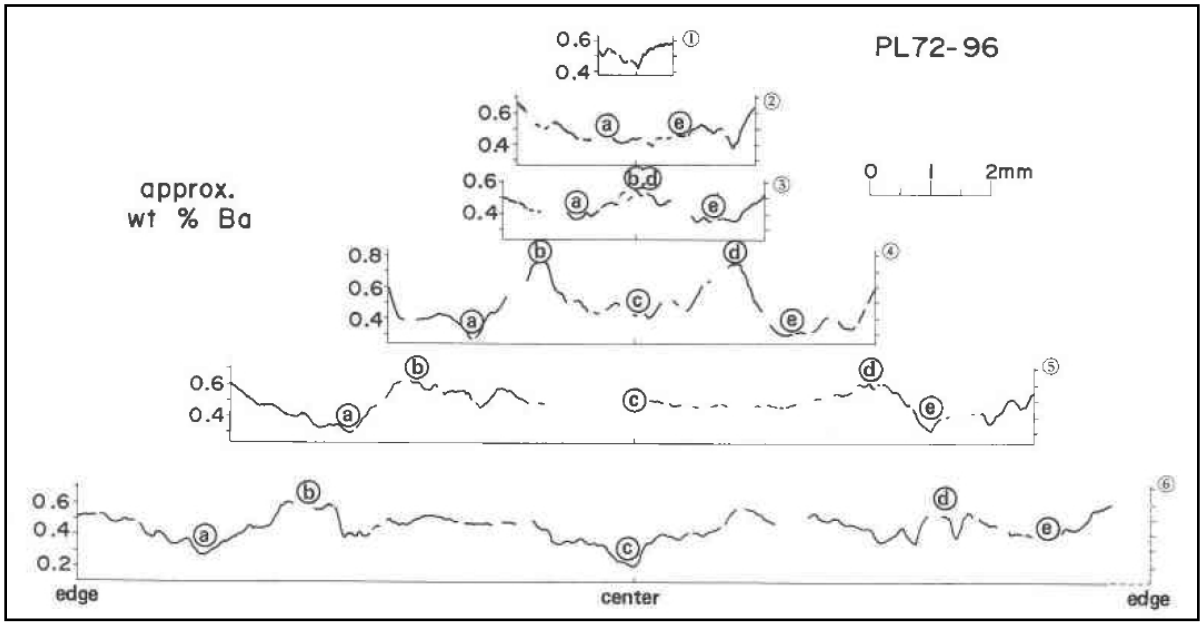

Figure 2.4. Image from Long and Luth (1986) of K-feldspar megacryst traverse data, which shows peaks of Ba. The concentrations of Barium increase as the size of megacryst decreases. The size of the crystal relates to the relative age, where younger crystals are smaller.

This project focuses on the crystallization history of the megacrysts and potential for evidence of magma mixing of the Halifax Pluton. To define a more accurate relative age range in the megacrysts of Peggy's Cove granites we use textural and chemical analyses of potassium feldspar (K-feldspar) crystals.

Megacrysts of the granite in the Peggy's Cove area are commonly 4-5 cm in length and 1-2 cm in width, and are euhedral to subhedral. In this research, because of the size of phenocrysts, the crystals will be referred to as megacrysts. Euhedral to subhedral grains suggest that the crystals crystallized under magmatic megacrystic conditions with little to no evidence of metamorphism, which also suggests magma transport, rather than metasomatism or regional tectonic activity (Vernon & Paterson, 2008). Large K-feldspar crystals that crystallize or are replaced by other minerals by metamorphic processes tend to have subhedral to anhedral shapes

as a result of reactions and ongoing local tectonic stress. To distinguish an igneous, magmatic origin, features such as Carlsbad twinning, oscillatory zoning and plagioclase inclusions within a euhedral structure are recognizable in K-feldspar (Gagnevin et al., 2008; Vernon & Paterson, 2008). Cox et al. (1996) demonstrated that the nature of mantled and non-mantled megacrysts can determine the fluid flow that surrounds the crystal during transport within the magma and whether or not that composition is the same as that of a crystal that formed in situ. The age of the mantled events does not explain when the crystal started to form, and research suggests that trace elements, such as barium (Ba) and strontium (Sr), give more conclusive evidence as to the relative age of the crystals (Cox et al., 1996). Therefore, chemical variations within K-feldspar megacrysts can be used to document the evolution of the granitic magma during their crystallization. For example, the incompatibility of Ba and the compatibility of Sr in a ratio can be used to indicate the stage of fractionation. Higher concentrations of Ba may indicate the start of nucleation in a magmatic setting, whereas higher Sr may indicate the final stage of growth or a sequence of re-melting (Cox et al., 1996; Vernon & Paterson, 2008).

The two-feldspar geothermometer is used to find the temperature at which two phases of feldspars (eg. K-feldspar and plagioclase) were in equilibrium. This is accomplished by calculating the feldspar constituents of the K-feldspar megacryst (Putirka, 2008). The calculation then uses a function that incorporates the feldspar composition into a pressure sensitive equation of experimental crystal growth. The data derive a temperature from selected experimental controlled environments such as Elkins and Grove (1990).

Chapter 3: Methodology

3.1 Introduction

A number of specific techniques were used to understand the petrology of the Peggy's Cove megacrysts, including: hand-sample descriptions; thin-section petrography; microprobe analysis, and cathodoluminescence.

3.2 Field Methods

3.2.1 Sampling

At the sites of the study, Peggy's Cove and Prospect, outcrops were selected with less superficial weathering and a substantial amount of megacrysts. Dykes and veins were avoided while searching for a representative sample of the area. Xenoliths were not avoided, in order to allow an understanding of the relationship between megacrysts and potential magma mingling.

3.3 Petrology

Samples were cut with a 10–inch diameter rock saw blade: this was the only blade that was large enough to slice larger samples. For smaller pieces of the sample already cut into a manageable size (small enough for a 6" saw), a faster cutting saw was used. Slabs 2-3 cm thick were obtained to check for the presence of megacrysts in thin section. Measurements and images of all the slabs were taken, and of the hand specimens.

Areas on samples from both study sites, (PC and PA) were selected for thin sections (polished and non-polished). The polished sections were chosen based on the presence of a complete sub-euhedral megacryst within the field of the thin section. Those with surrounding matrix were more favourable. Two samples from PA megacrysts were chosen ('A' and 'B') to get

a representation of change through the third dimension of the rock. The PC sample megacrysts were fewer and less euhedral in the third dimension, so only one section of this sample was chosen. The larger thin sections were chosen to observe the megacryst in the matrix, the composition of the matrix, and influence the matrix has on the megacrysts (see Fig. 3.1).

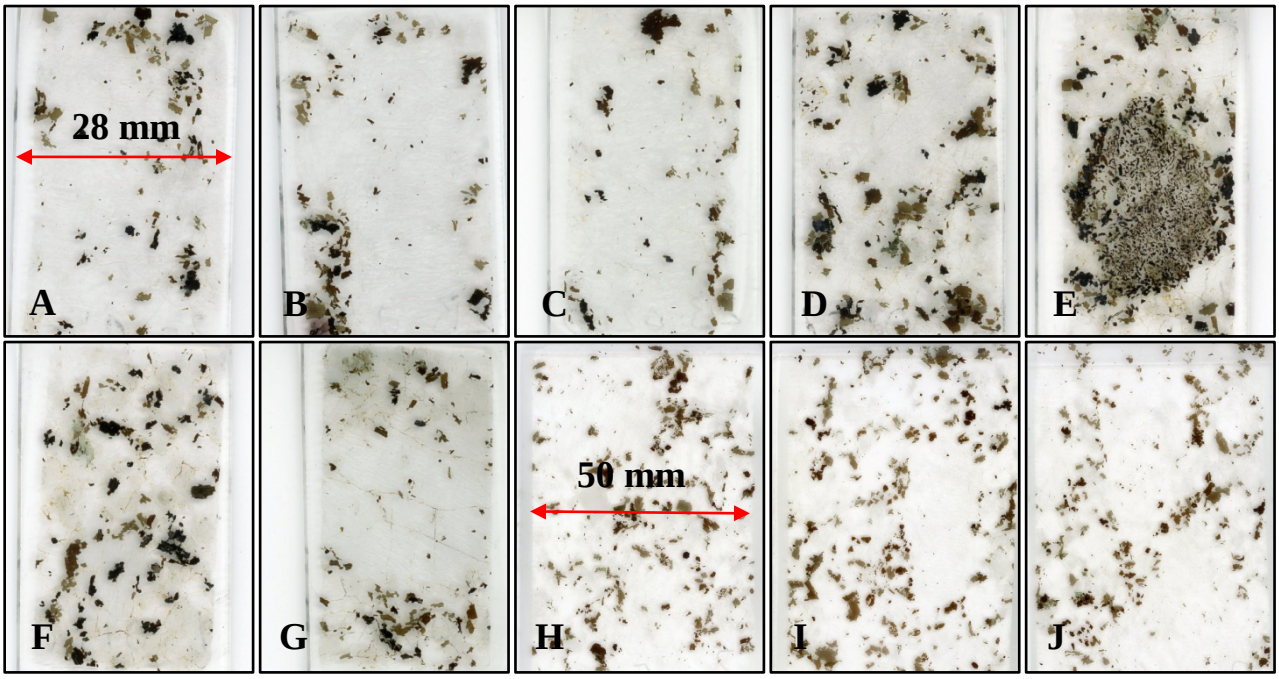

Figure 3.1. A series of images of the cut samples. Most thin sections show large empty spaces, which are K-feldspar megacrysts. The thin sections have the following dimensions: from A to G, 27 mm by 48 mm, and from H to J, 50 mm by 75 mm.

3.3.1 Microscopy

Microscopy was performed on a Nikon ECLIPSE 50iPOL. A digital camera was used to capture images. Because the megacrysts are larger than the field of view, multiple overlapping images were obtained to create a complete map of the megacryst in thin section. Each image is taken in careful relation to the previous image, with a suitable amount of overlap.

3.4 PTGui

3.4.1 Operation of PTGui

PTGui is a photo stitching program. Images that are adjacent or in a sequence can be used to create a larger collage. If there are images that do not align properly, the user must create control points in the adjacent images to form a relationship.

3.4.1 Application of PTGui

The images collected from the microprobe were joined to create panoramas with the two sets of dimensions (width x height) ~7000 by ~15500 or ~13500 by ~15500 pixels. Photographs in cathodoluminescence (CL) that are adjoined have the sets of dimensions (width x height) of ~11000 by ~9000 pixels and ~8500 by ~10500 pixels. Each panorama was created using 30 to 100 images.

3.5 Cathodoluminescence

3.5.1 Background of cathodoluminescence microscope

Cathodoluminescence is a method used to excite electrons, causing electrons to emit in the visible range of the electromagnetic spectrum. Typically the colour radiated is unique in minerals (McLemore & Barker, 1987). Factors that can change the resulting colour are mineral impurities, instrument conditions, and the viewer's colour perception. In this way, physical and chemical phases can be identified using cathodoluminescence, but care must be taken in interpretation(Slaby & Gotze, 2004).

Research by McLemore (1987) indicates the uses of cathodoluminescence can identify growth rings, overgrowths, intergrowths, and healed fractures. Zoning shows the cycles of nucleation and may vary in size and shape.

3.5.2 Operation of cathodoluminescence microscope

The HC4-LM Cathodoluminescence Microscope (CL) was used at Saint Mary's University. To avoid electrical charging of the thin section, the slides can be coated in gold or carbon; this research used carbon. The coating was completed at Dalhousie University at the time of selecting areas for thin section. The polished surface faces downward in the CL as the beam passes through the entire thickness of the sample. The magnification of the CL is at 5X.

3.6 Electron Microprobe

3.6.1 Operation of electron microprobe

The JEOL JXA-8200 Microanalyser (EMP), 'SuperProbe' is located at Dalhousie University. The EMP is a probe with five wavelength-dispersive X-ray spectrometers (WDS) and has an additional energy-dispersive X-ray spectrometer (EDS). The microprobe is capable of analysing surfaces as small as 0.1 µm. The equipment is able to detect a range of a few parts per million (ppm) to several hundred ppm for most elements common in silicate minerals. This device is capable of detecting most of the elements (Be-U) and 21 elements simultaneously. The method that EMP incorporates is the bombardment of a polished sample with electrons; the EDS detects the resulting energies, and the WDS distinguishes wavelengths of interest (JEOL, 2012). These detection methods convert volumes into concentrations of elements, which can then be correlated with the standard plates. The relationship between the sample and the standard is the count of the resulting x-rays. The x-rays are calculated by finding the unknown concentration (conc.) of the sample in the following formula as summarized by McCuish (2001):

$$\frac{counts\ \ on\ sample}{conc\ .of\ \ sample\ _{unk}} = \frac{counts\ \ on\ standard}{con\,c.of\ \ standard} \qquad (3.1)$$

The microprobe indicates concentrations of various major and trace elements and converts them to oxides for the printout. The oxides that are most useful in this research are SiO_2, Al_2O_3, FeO, MgO, MnO, Na_2O, K_2O, CaO, BaO, SrO and Eu_2O_3.

3.6.1 *Mineral Analyses*

The selected crystals for the microprobe have a euhedral shape, are large, with exsolution lamellae and have concentric inclusion trails that were trapped along the growing faces of the developing megacryst. The inclusions therefore represent mineral phases that can be considered as having grown in equilibrium with the megacryst. The standards were collected according to the projected element.

3.6.2 Point analyses

A 200x200 pixel area (4mm^2) was chosen for a number of point analyses, each pixel has had the dimensions 20x20 microns (µm). An additional 200x150 pixel area with pixel dimensions of 20x20 µm was selected for more detailed analysis. The electron beam moves in a line across the sample when taking a line scan of the megacryst.

3.6.3 Backscattered electron (BSE) imaging

Two samples were selected for backscatter imaging, samples 2a-05a and 4a (1-04a). The sample 2a-05a is a representation of Prospect area and 1-04a is from Peggy's Cove. The exsolution map for sample 2a-05a was set with the dimensions 500 x 500 pixels, a five micrometer pixel size and a 20 millisecond (ms) dwell time. There is 30 points in total count: five points for the host K-feldspar, six for the coarse perthite, six for the plagioclase inclusion, seven for another part of the host K-feldspar and six for the fine perthite (Fig. 3.2).

The exsolution map for sample 4a (1-04a) has the same settings as the 2a-05a exsolution map. There is a total of twenty one points of analyses in 4a, six in the plagioclase inclusion; five in coarse perthite and in (two) host K-feldspar.

3.6.4 X-ray mapping

The initial beam settings are 15 eV at 100 nA. The dimensions are set for 700 * 500 pixels (l*h) with each pixel 30 * 30 µm and a 20 ms dwell time. The start point was 3.6317, 71.3799, 10.1220 mm (x, y, z).

3.7 ImageJ

3.7.1 Background Information

ImageJ is digital imaging freeware (public software) created by the Research Services Branch (RSB) of the National Institute of Mental Health (NIMH). The program is used for particle analysis; spatial calibration; processing and analyses of raster data.

3.7.2 ImageJ Operation

After cropping and converting the microprobe images to grayscale, there were five steps performed: 1) setting the scale; 2) excluding pixels; 3) changing the threshold values; 4) making the image binary; and 5) analyse particles in ImageJ.

The scale of image units is in the default setting and need to be changed to microns, and cross-referenced by a known length. This process defines the dimensions of the image. Cropping inclusions and empty space from the image decreases the deviation. Excluding the pixels is the process required to get an accurate percentage in the results. The threshold is the method for increasing the contrast between light and dark aspects of the image. By increasing the contrast, the host crystal becomes more distinct from its lamellae. Changing the image into binary is a process to increase contrast further. Making an image binary, the method leads to two results. The results of the binary operation are two levels, zero (black) and 255 (white) show the contrast of the selected areas for analysis. Analysing particles create a numerical summary in the text of the binary results. This final action takes the ratio of one out of the sum of both results from the binary image.

Chapter 4: Results

4.1 Introduction

The techniques utilized in the data collection for Peggy's Cove and Prospect samples were selected to distinguish compositional changes within this phase of the magma of the Halifax Pluton. To test the hypothesis that there was more than one magma present, as the result of differentiation during the crystallization of the PC and PA megacrysts, supporting evidence must be found. Barium concentrations, two-feldspar geothermometry, and supporting microprobe data are potential tools for interpreting results. Petrography from this study agree with previous work of the Halifax Pluton by MacDonald et al. (1992) and MacDonald (2001). These granitoid rocks of both sample areas are biotite monzogranites. Peggy's Cove has an intermediate colour scheme and an overall darker hue, whereas PA has a lighter colour, which is a result of higher amounts of visible K-spar megacrysts and feldspar aggregates (Fig. 4.1).The modal proportions are: K-feldspar is 25-35%; quartz is 20-45%; plagioclase is 15-25%; biotite is 10-17%. The grain size of the biotite monzogranite in Peggy's Cove is observed to be smaller overall than Prospect Area and is exhibited in biotite grain sizes.

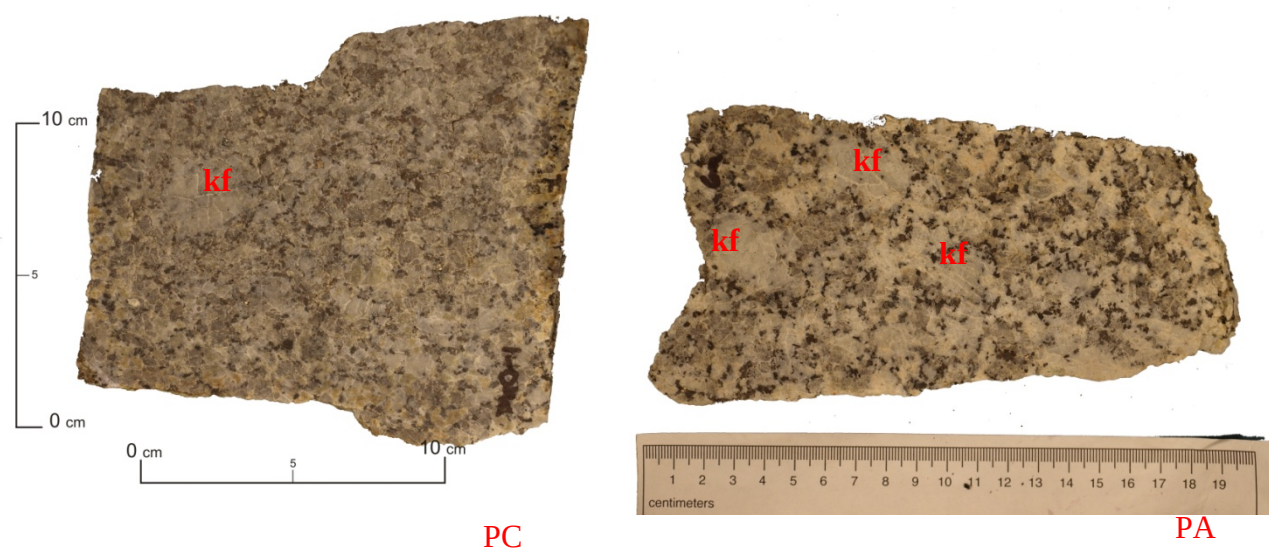

Figure 4.1. A series of images from sample areas, Peggy's Cove and Prospect. These are 2 out of 55 selected images (PC is on the left and PA is on the right).

4.2 Peggy's Cove

Peggy's Cove outcrops show rust-coloured staining near the surface and in fractures, whereas Prospect Area outcrops have a rust colour throughout the matrix, but more near the exposed margin, possibly reflecting slight differences in overall mineralogy. Overall, the rock has a brownish-grey colour. On closer inspection, the hues of the matrix are light grey, dark grey and black.

4.2.1 K-feldspar

The K-feldspar megacrysts have various size ranges from 3 cm x 1.25 cm to 2 cm x 0.75 cm and K-feldspar also form aggregates with plagioclase within the matrix (Fig. 4.1). The K-feldspar aggregates are difficult to differentiate from other light coloured minerals in the matrix.

4.2.2 Plagioclase

The plagioclase has various shades of grey, but is mostly smoky grey. The texture of plagioclase is massive within the hand sample.

4.2.3 Biotite

Biotite is black and in the form of flecks. Biotite is commonly found in patches and forming small enclaves. The grain size range for biotite is 0.1 - 1 mm.

4.2.4 Quartz

Quartz has varied size anhedral grains ranging from 1-5 mm, is typically interstitial and is a smoky grey colour.

4.2.5 Other features

There is a presence of a dark coloured, aphanitic xenolith within the matrix (Fig. 4.2 a). On closer inspection the xenolith appears to be two sets of biotite, one set is observed to be comprised of dark brown, anhedral grains with a reaction texture; the other set exhibits a range of yellow to brown sub-euhedral grains (Fig. 4.2 b).

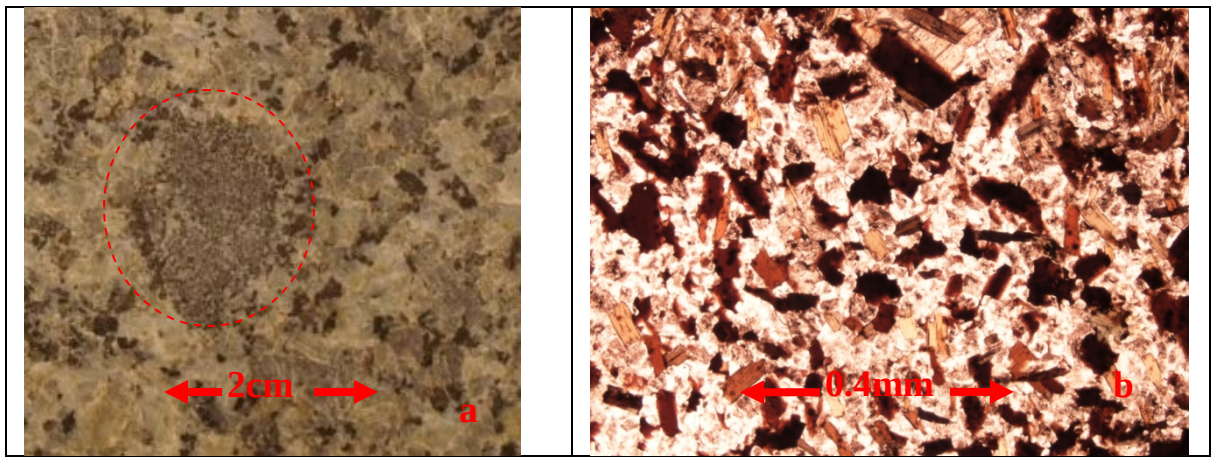

Figure 4.2. A photo of a xenolith found within the PC site (1-012a). The remnant has a ~2 cm diameter. The right image is observed to be an aggregate of biotite and plagioclase.

4.3 Prospect Area

The PA sample has an overall lighter hue than PC, and is white and brown with grey mottling. The megacrysts are more defined than in the PC, and the textural contrast, as well as the hue contrast between different minerals makes it easier to identify grain boundaries within this granitoid (Fig. 4.3).

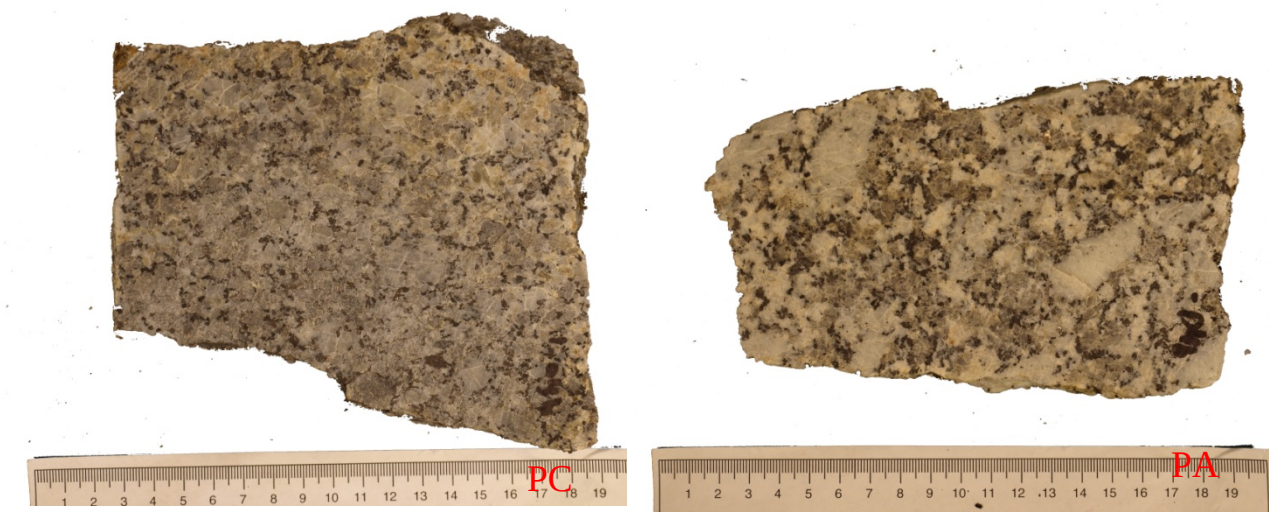

Figure 4.3. A image that demonstrates the textural difference between both sample areas.

4.3.1 K-feldspar

The K-feldspar of the PA sample has a euhedral shape when in the form of megacrysts. The megacrysts range from 4 x 1.5 cm to 2.5 x 0.75 cm (length by width). Twinning is visible on larger crystals under good lighting conditions. Overall, the megacrysts found in the PA sample are larger than the PC sample megacrysts.

4.3.2 Plagioclase

Plagioclase occurs predominantly within the groundmass, has a massive texture in hand sample, and is difficult to distinguish from the K-feldspar massive texture in the groundmass.

4.3.3 Biotite

The biotite grains are throughout the matrix. Few of the biotite crystals can be found within the megacrysts, but are typically situated around the margins of the megacrysts. When associated with the megacrysts, matrix biotite crystals tend to accumulate on one side rather than all sides, although, there is no preference for a particular side from grain to grain. This texture is consistent throughout the individual slices of the whole rock surface (Fig. 4.4). The PA sample has a grain size range of 0.5-3 mm.

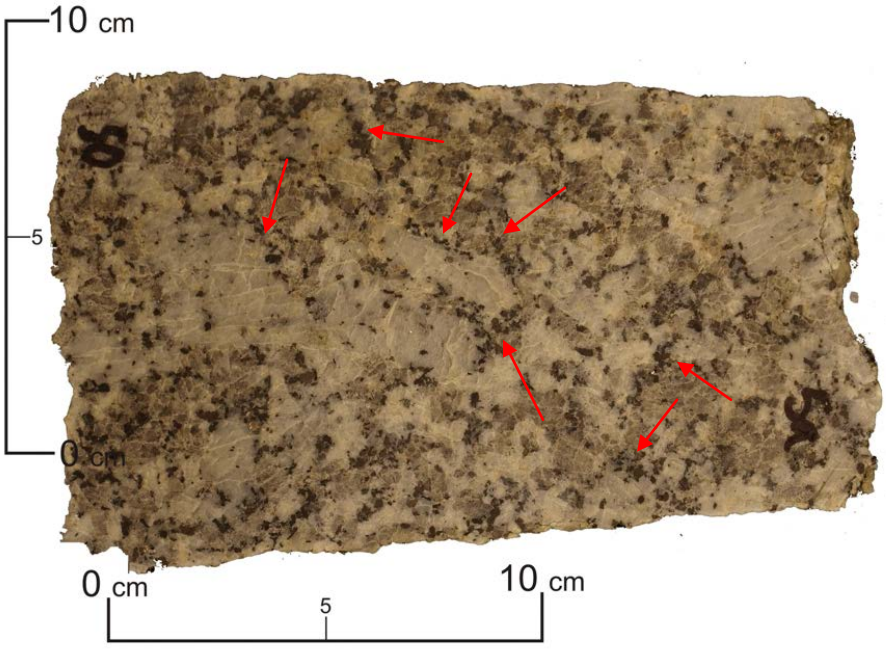

Figure 4.4. A sample from PA that shows accumulations of biotite indicated by red arrows. The arrows point into the bands of biotite. Note that these are not all in the same orientation.

4.3.4 Quartz

The mineral quartz is a smoky grey colour making it easier to distinguish from the K-feldspar and plagioclase in hand sample. The crystal grain sizes vary within the ground mass. In the PA sample, the quartz grains are larger than PC quartz grains. In the PA, the average grain size range is 3-7 mm. There is less quartz in the PA sample than in the PC sample.

4.3.5 Other features

There is an autolith in the sample (a) that is observed to have approximately the same mineral proportions as the host rock with a finer grained texture (Fig. 4.5). In addition, it is not uncommon to find enclaves of biotite present in the host granitoid (4.5 b).

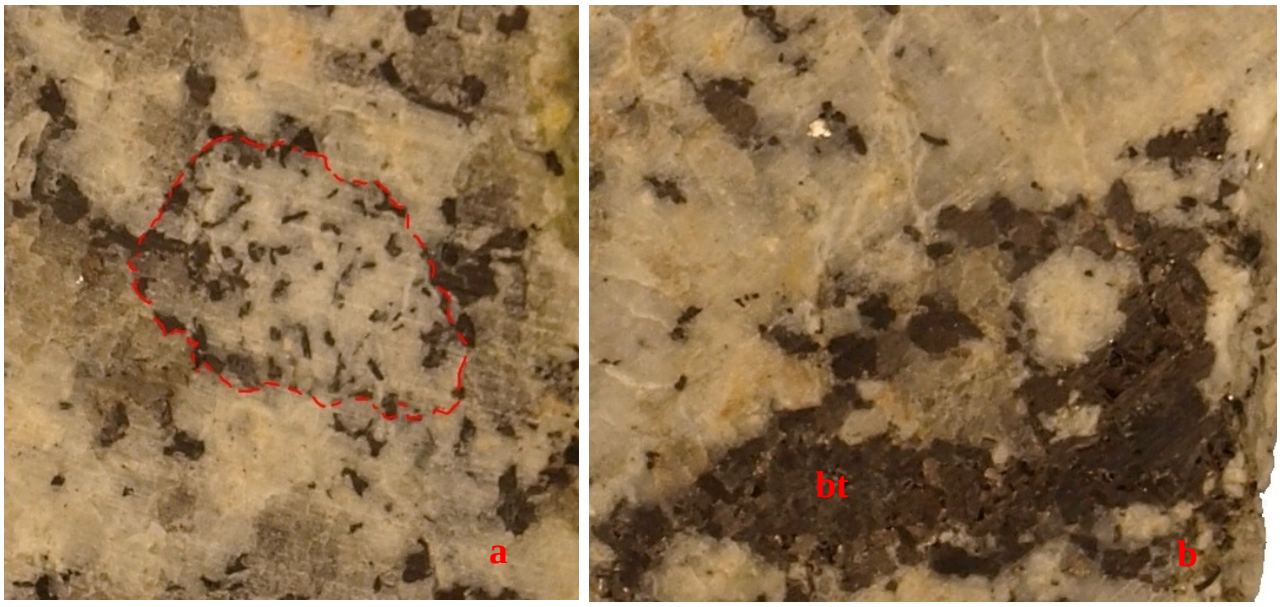

Figure 4.5. Two photographs, the one of the left (a) is the observed autolith, about 1.5 cm in diameter; on the right (b) is the biotite enclave which is 3 cm length-wise. The autolith is outlined in red to distinguish the shape from the groundmass, areas of the margin indicate assimilation.

4.4 Petrography

4.4.1 Petrographic Description

Descriptions for both sites are combined in this section. When using microscopy, the sites have similar mineralogical features and show little differences in microscopic scale.

4.4.2 Megacryst

K-feldspar shows exsolution textures, a larger perthite with smaller perthites that overlap (Fig. 4.6). The perthite is observed to be perpendicular to the long direction of the crystal host. There are several inclusions of biotite and plagioclase that form crystal boundaries along the megacryst edge.

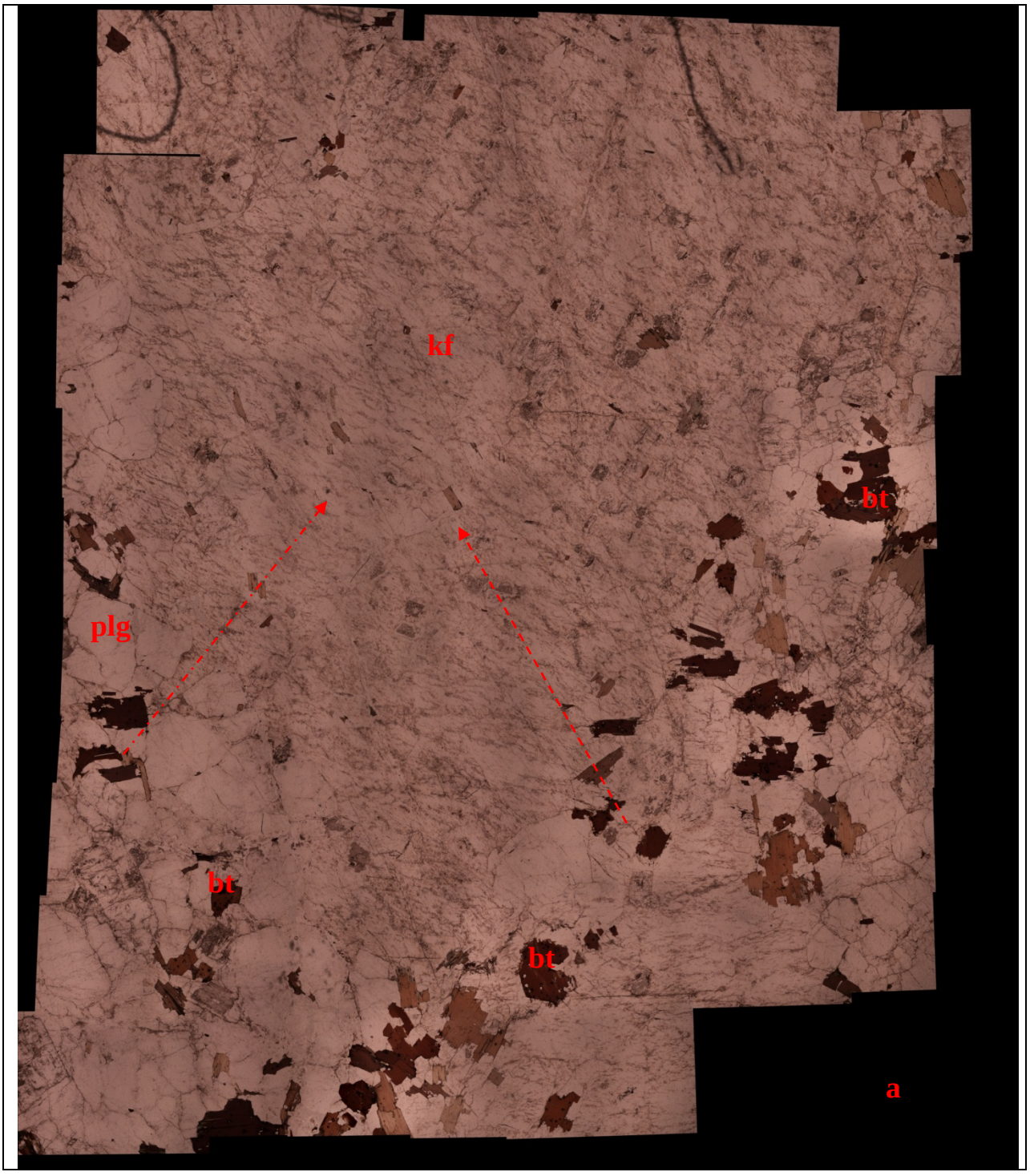
kf
bt
plg
bt
bt
a

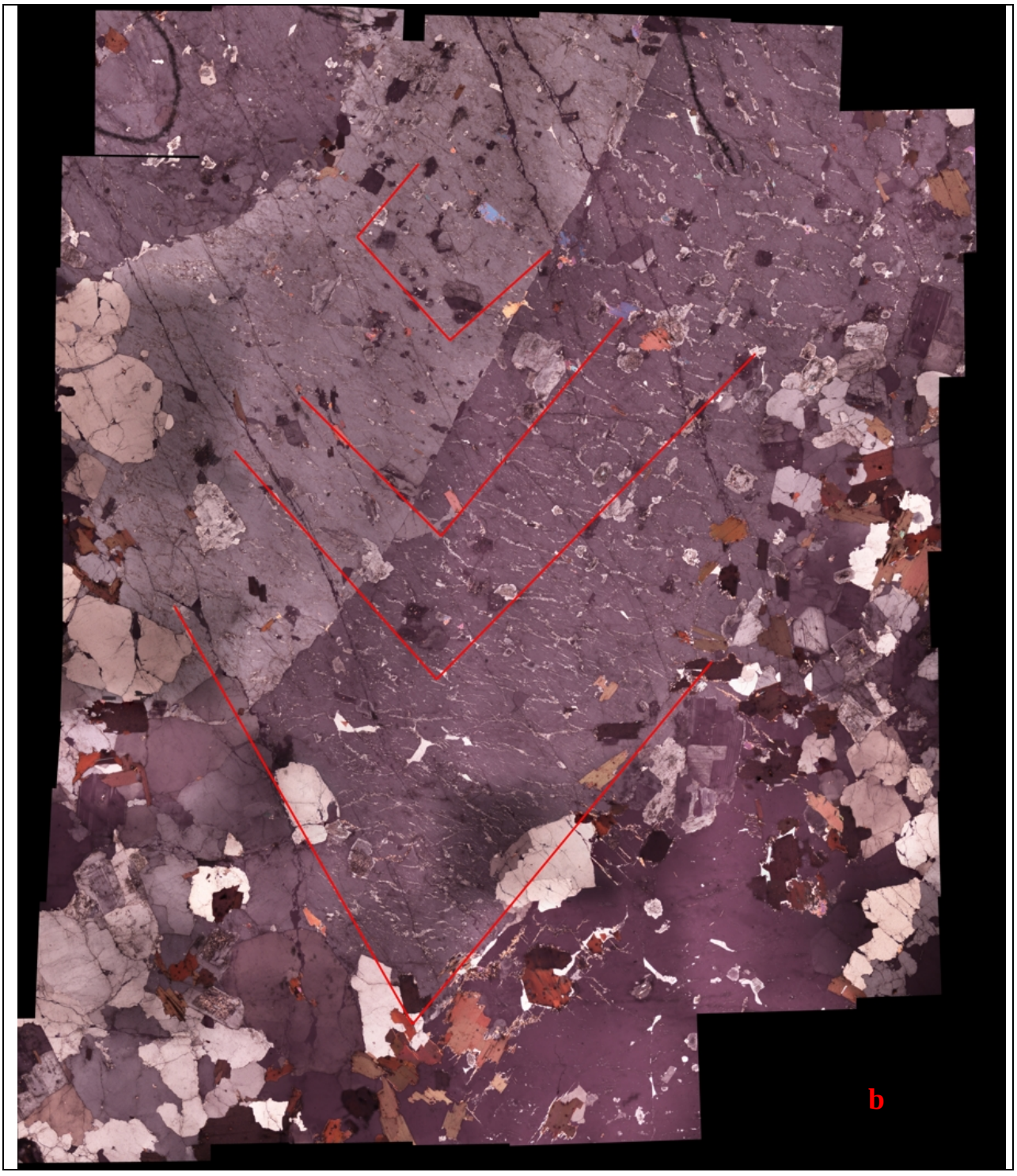

Figure 4.6. A megacryst from Prospect area that is compiled as collage from a number of high resolution photographs taken in PPL and XPL by Nikon ECLIPSE 50iPOL microscope. In the upper image (a), directional arrows signify the decreasing size of biotite. In image (b) the plagioclase and biotite inclusions are arranged in a concentric pattern (growth boundaries).

4.4.3 Inclusions

In Figure 4.7 (a), plagioclase and biotite crystals are in arrangements that indicate growth stages of the megacryst; the plagioclase that is within these features show several characteristics: zoning, twinning, sericitic and myrmekitic texture (see Fig. 4.7 b-e). Some biotite crystals inside the megacrysts show a slight reaction texture. This reaction is reflected by a change of colour from dark cores to lighter rims in the biotite crystals (Fig. 4.7 f).

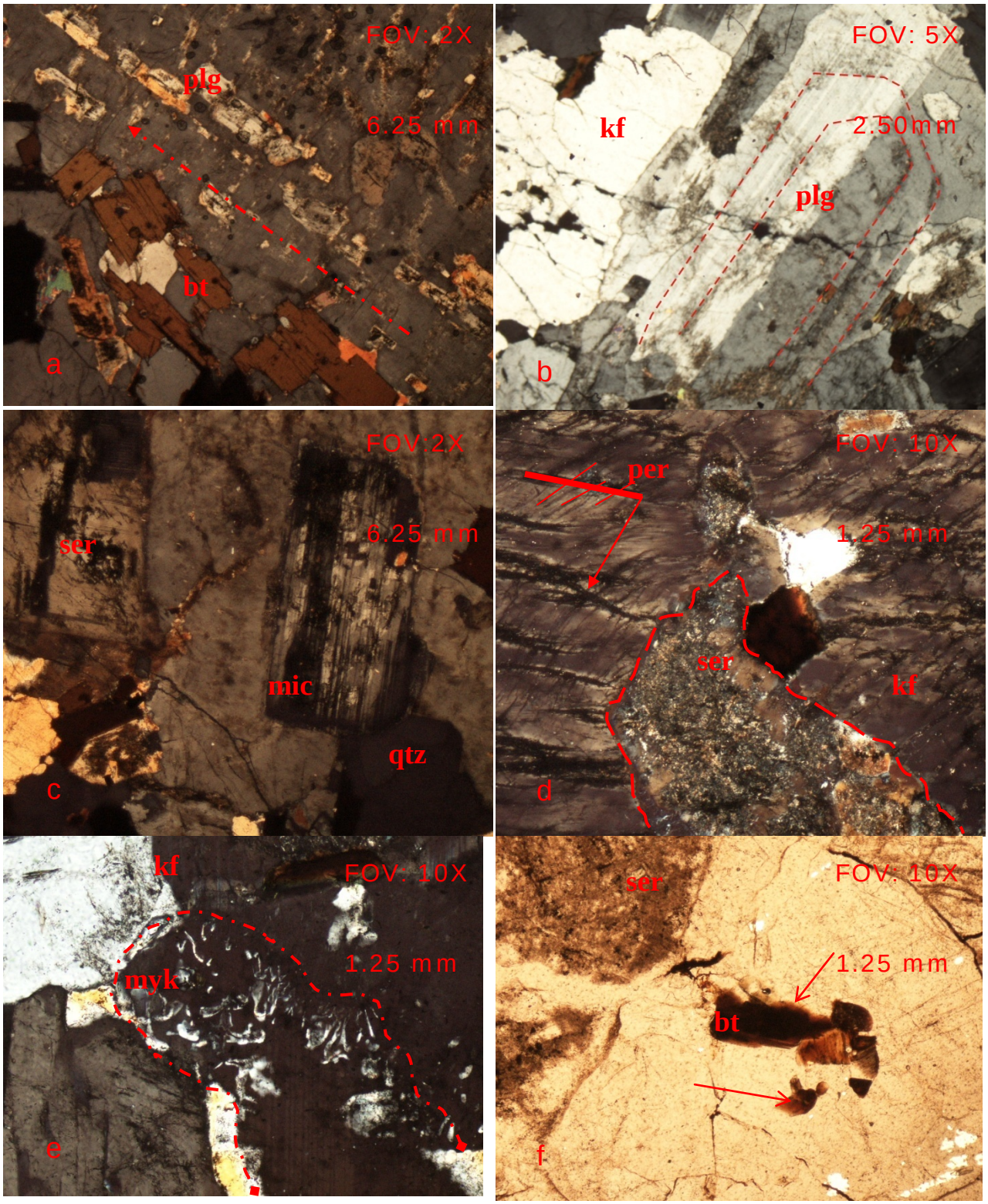

Figure 4.7. A series of images from both sites that are observed to have various textures and orientations. Image a) shows a inclusion trail indicated with a arrow; b) is an example of oscillatory zoning in plagioclase is indicated by broken outline; c) shows secondary reaction texture microcline (mic); d) shows large perthite (per) crossed by smaller perthite lamellae and large area of sericite (ser); e) indicates a margin of myrmekite (myk) indicated by outline; f) shows arrows pointing to melt textures on a grain of biotite.

4.4.4 Mineral Description

The overall textural description of each mineral phase within both sites is described in this section. Distinguishing features will be further discussed in Chapter 5.

4.4.4.1 K-feldspar

In plane polarized light, K-feldspar looks dirty (Fig. 4.6 a), in crossed polarized light (XPL) the separated perthite are the 'dirty' regions. Secondary textures are observed in XPL, such as myrmekite, a texture found near the contact margin of K-feldspar and plagioclase (Fig. 4.7 e).

4.4.4.2 Plagioclase

In PPL, plagioclase shows less incipient alteration and no exsolution in comparison to K-feldspar. Plagioclase looks similar to the K-feldspar crystal, it is slightly clearer due to the absence of perthite exsolution lamellae (Fig. 4.6). Plagioclase in XPL is of two types: inclusion and primary growth. The inclusion type is found within the crystal structure of K-feldspar, these plagioclase crystals have a zoned edge with a sericitic texture toward the core (Fig. 4.7 c). There are areas of microcline on the plagioclase grains.

4.4.4.3 Biotite

Biotite inclusions shows a decreasing grain size toward the core of the megacryst (Fig. 4.6). Grains of biotite observed under microscope in XPL have pleochroic haloes (Fig. 4.7 a).

4.4.4.4 Quartz

Quartz exhibits an anhedral shape with undulatory extinction (Fig. 4.7 c).

4.5 Cathodoluminosity

4.5.1 K-Feldspar

The results of K-feldspar after the emitted light from the cathodoluminescence show slight colour variation due to chemical zoning. The remnant crystal phases are indicated by alternating lighter and darker hues within the megacryst (Fig. 4.8 PC). Some remnant features, such as zoning are easier identified by observing trails of plagioclase inclusions (Fig. 4.8 PA).

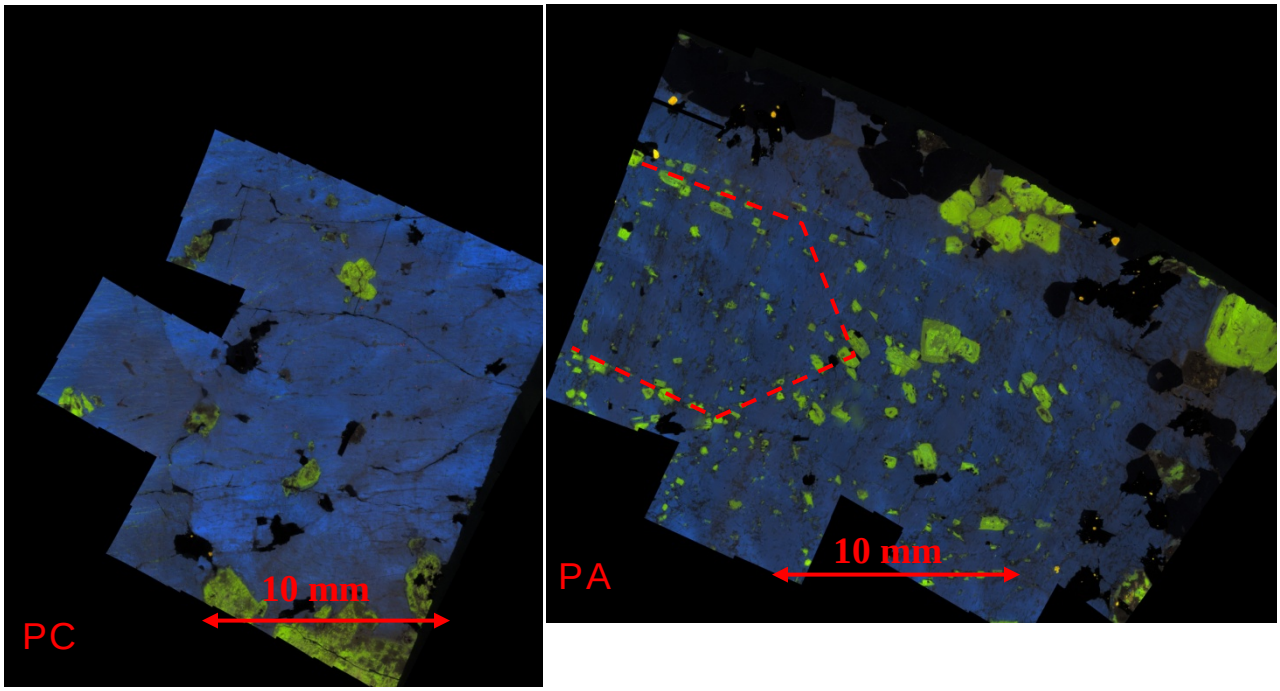

Figure 4.8. Two CL photographs (collaged) of megacrysts from both sample sites. Each single image was captured at 5X (FOV). The broken line in the PA image outlines plagioclase grains that are in a remnant structure.

4.5.2 Plagioclase

Plagioclase is observed as green in CL. Inclusions of plagioclase are common in PA megacrysts and can be observed forming remnant rim patterns (Fig. 4.8). Typical grains of plagioclase in the samples have euhedral to sub-euhedral shapes. The plagioclase with noticeable zoning are the inclusions within the megacrysts.

4.6 Electron Microprobe Analyses

4.6.1 K-feldspar Mineral Chemistry

The results of the point analyses taken along a transect from the interior of the megacryst show that the megacrysts record variations in both major and trace element compositions. The graphs shown below (Fig. 4.9), represent BaO on the x-axis plotted against both trace (Sr, Mn, Eu, Fe) and major (Ca, Na, K, Al) elements. BaO vs Mn shows the samples from PC show more Ba content and a smaller variation in Ba than the samples from Prospect. In contrast, strontium and manganese concentrations are higher in the megacrysts from Peggy's Cove versus those from Prospect.

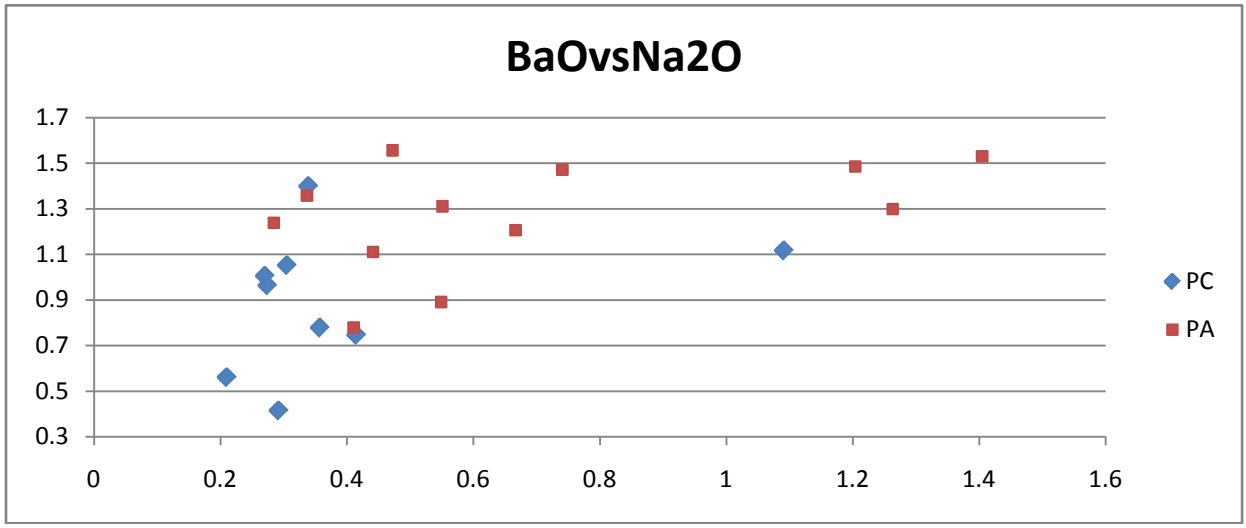

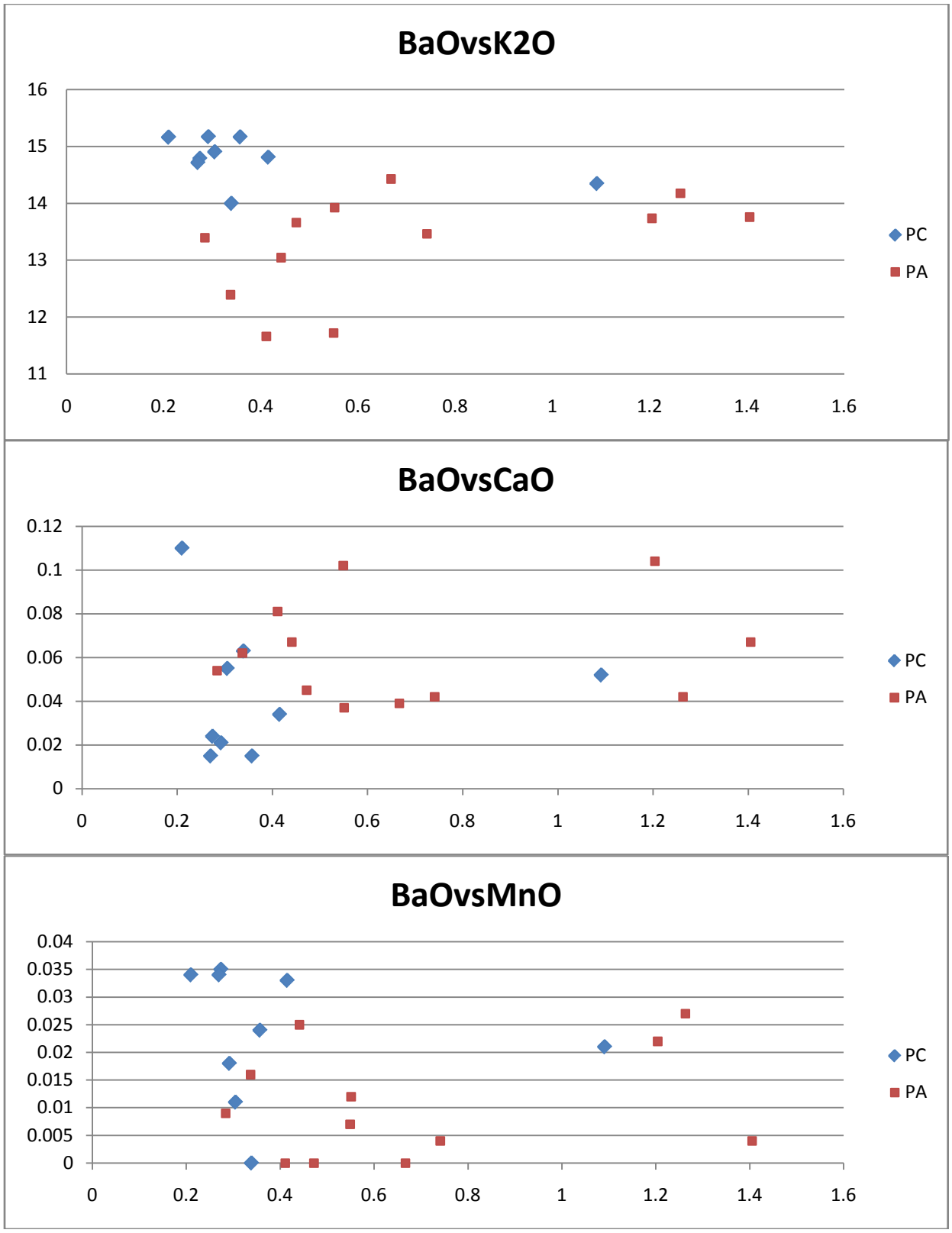
BaOvsK2O
16
15
14
13
12
11
0
0.2
0.4
0.6
0.8
1
1.2
1.4
1.6
PC
PA
BaOvsCaO
0.12
0.1
0.08
0.06
0.04
0.02
0
0
0.2
0.4
0.6
0.8
1
1.2
1.4
1.6
PC
PA
BaOvsMnO
0.04
0.035
0.03
0.025
0.02
0.015
0.01
0.005
0
0
0.2
0.4
0.6
0.8
1
1.2
1.4
1.6
PC
PA

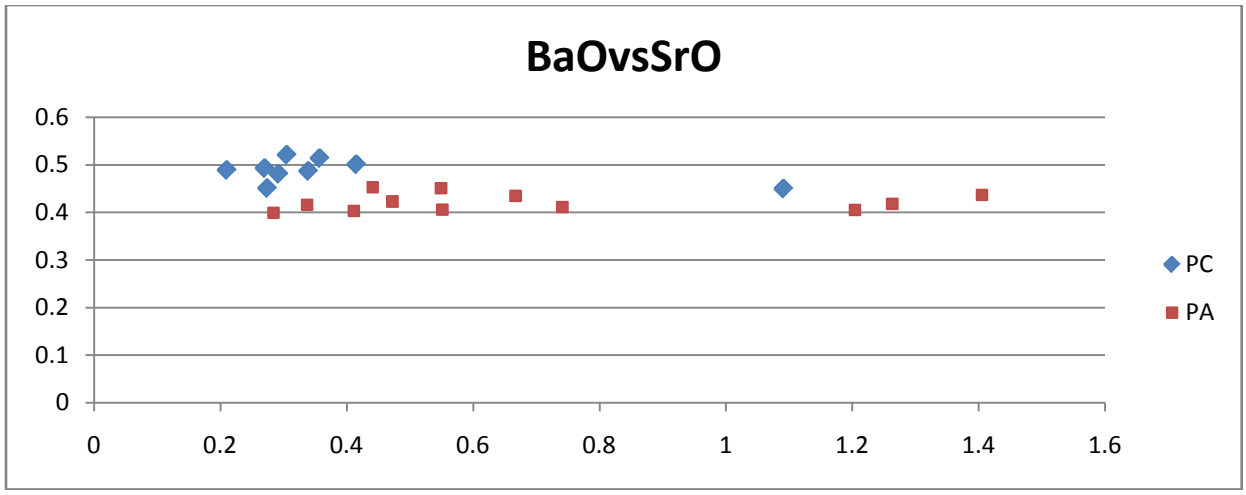

Figure 4.9. Barium plots that show BaO as the x-axis in comparison with a number of major and trace element oxides as the "y" component.

Barium line plots were produced in excel from the PC sample Ba core to rim transect results (Fig. 4.10). The 150 step image, the PC sample exhibits sequential peaks, which after ~2500 microns the peak occurs every 12,500 microns. In the 100 step image (PA), there are peaks between ~1500 to 2000 microns (refer to Appendix D for the line scan data).

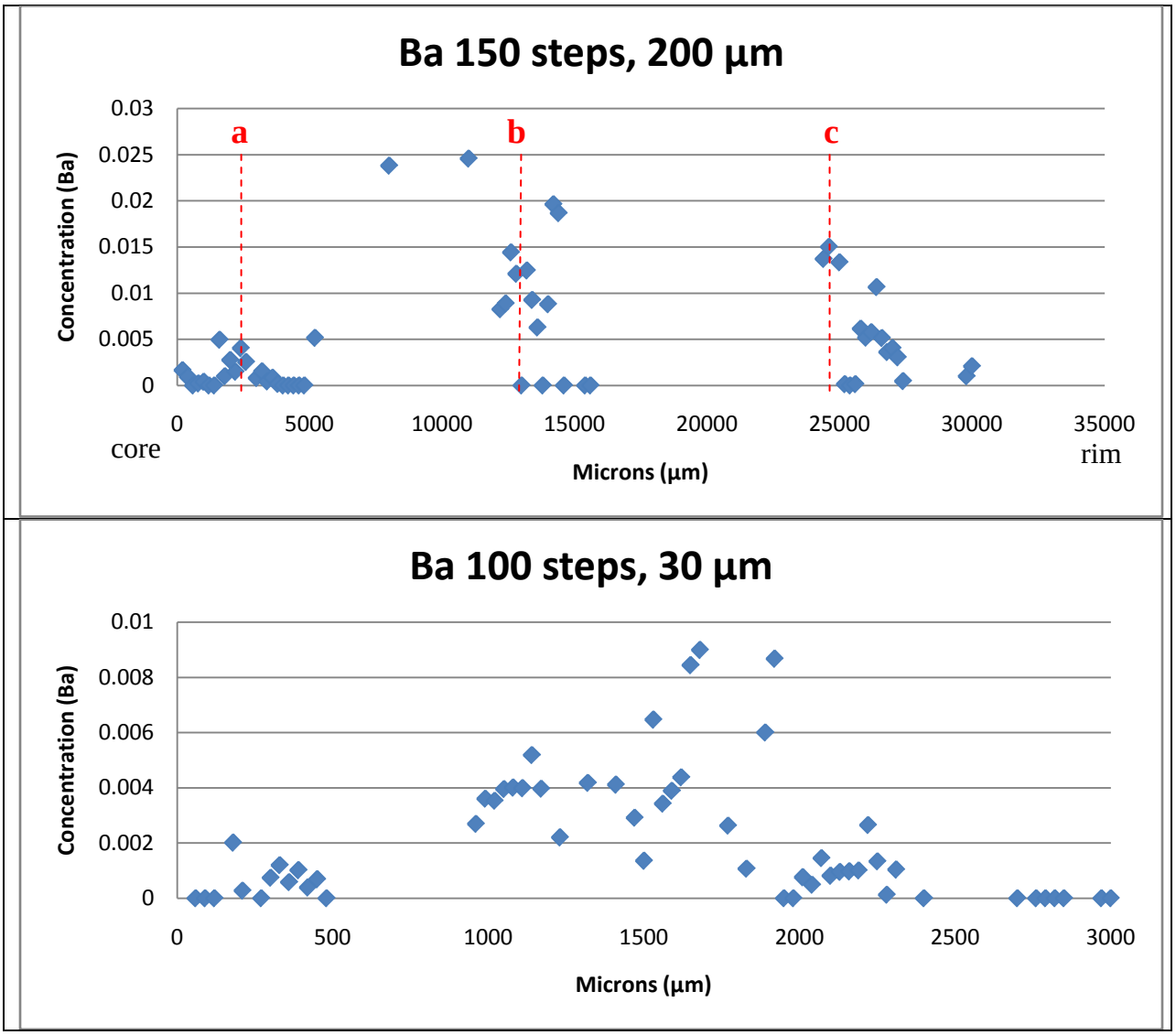

Figure 4.10. The step-lines, two diagrams of converted plot data. Both images show peaks in the data. The peaks are defined by broken lines in the PC sample. Whereas, the Prospect sample has one described peak.

Line data were also used to produce tri-plots (Fig. 4.11). The 150 point tri-plot exhibits the percent amounts of albite, anorthite and K-feldspar phases in the PC megacryst that were analysed during the step-line. The 100 point tri-plot indicates the phases in the Prospect sample.

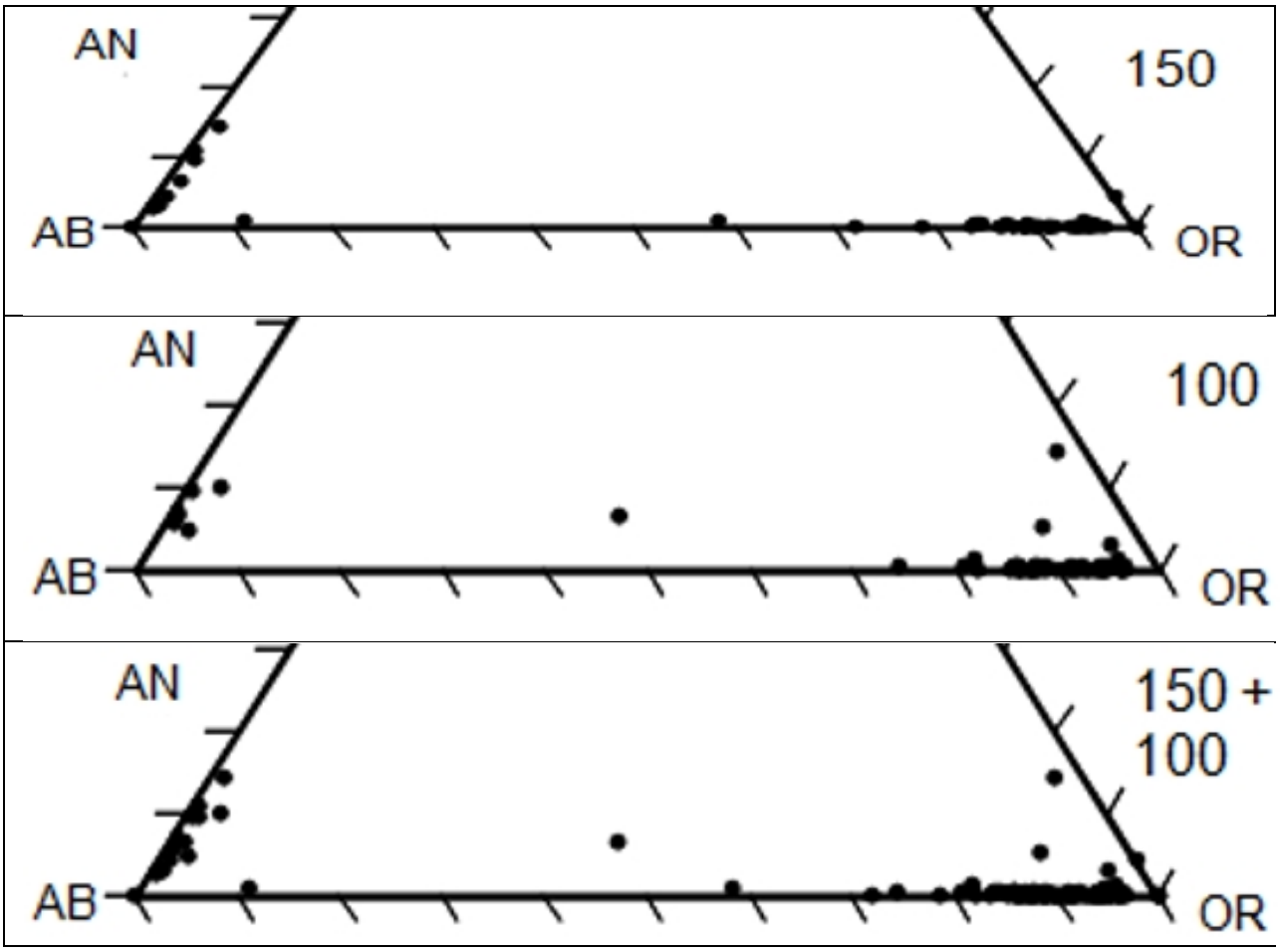

Figure 4.11. Three tri-plot diagrams at An_{30}that show the data of each point in the line scan, a) the 150 point; b) the 100 point; c) a hybrid of both a and b.

4.6.2 Element Maps

Figure 4.12 highlights the areas within a PC megacryst selected for detailed element mapping. These regions were selected because of features that were observed, these are a rim to core relationship; exsolution lamellae, and mineral inclusions.

-

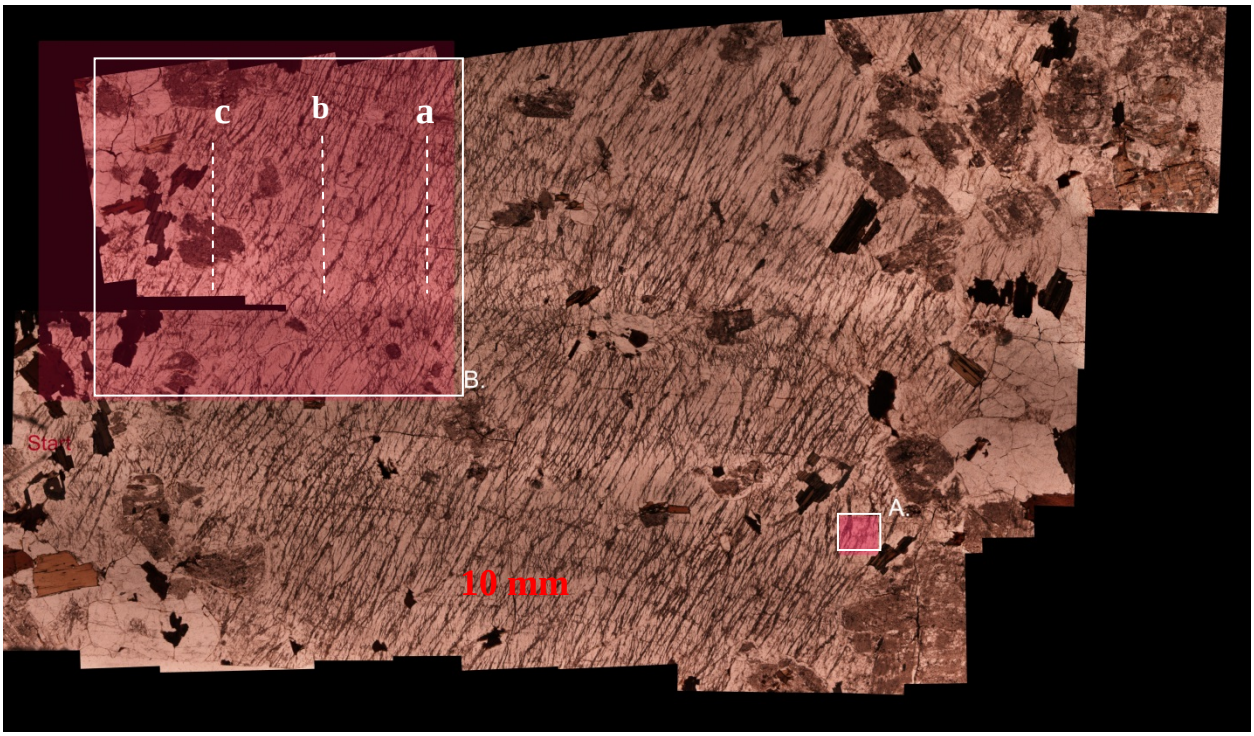

Figure 4.12 A microscopic image of the PC megacryst (1-04a). The red areas are the points of observation, A) is the area of the small map, and B) is a area of the large X-ray map. In B, the white broken lines are to identify the approximate barium peaks found in Figure 4.10.

The concentration of an element in a microprobe image is represented by a colour spectrum ranging from blue at the low end, to yellow, then to red at the high end. If none of the element in question is present the map is black (Fig. 4.13).

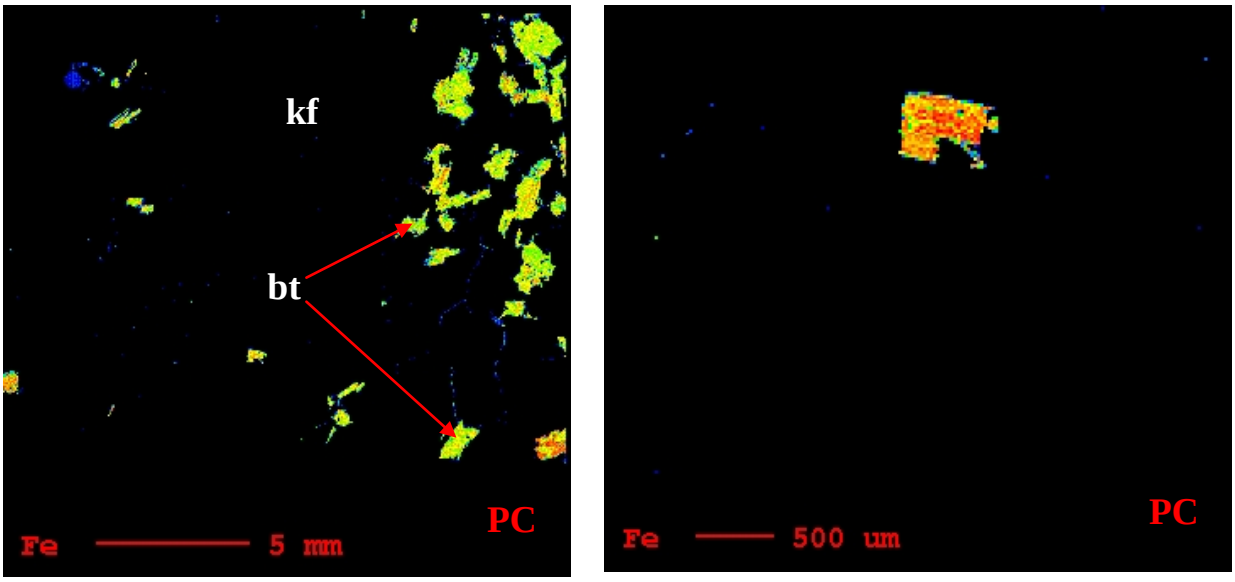

Figure 4.13. A generated microprobe image of Figure 4.13, section B. Iron is concentrated in biotite crystals and focused in the margin of the K-feldspar megacryst.

4.6.2.1 Iron

The element Fe is concentrated in the biotite crystals that are near the margins of the megacryst. There are few Fe-bearing inclusions within the center of the megacryst with the result most of the center is coloured black (Fig. 4.13).

4.6.2.2 Potassium

The element K is present in high concentrations in the K-feldspar in the images (Fig. 4.14). Another mineral with elevated concentrations of K is biotite with lesser K than the K-feldspar. The plagioclase show a low concentration of K, observed as a spotty blue colour on the maps (Fig. 4.14).

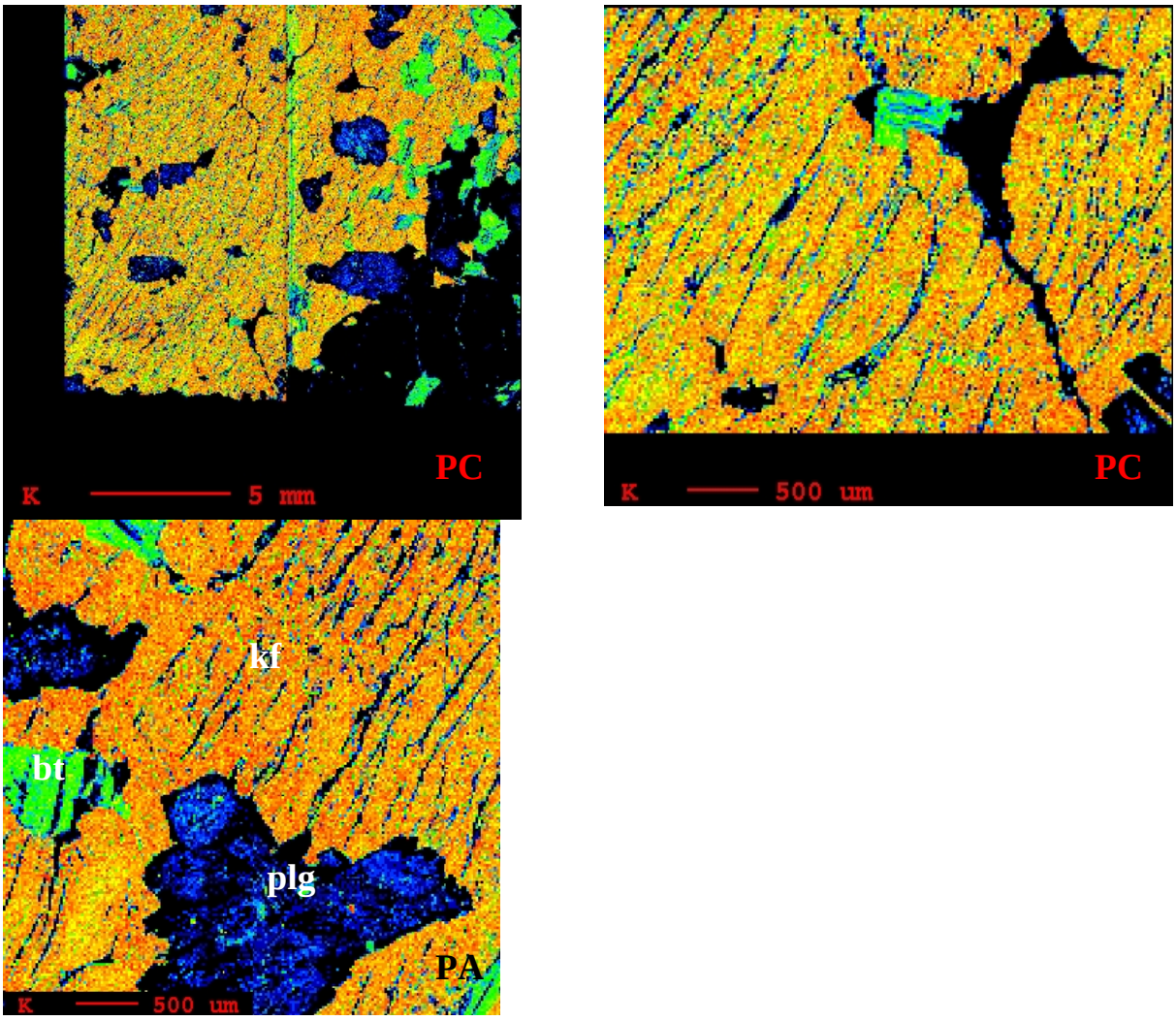

Figure 4.14. Three images from the microprobe that show the concentration of K. Potassium is present in low or none in exsolution lamellae and plagioclase (plg).

4.6.2.3 Titanium

The element Ti is found in trace amounts within biotite grains. There is titanium oxide present and it occurs in relation to biotite (Fig. 4.15).

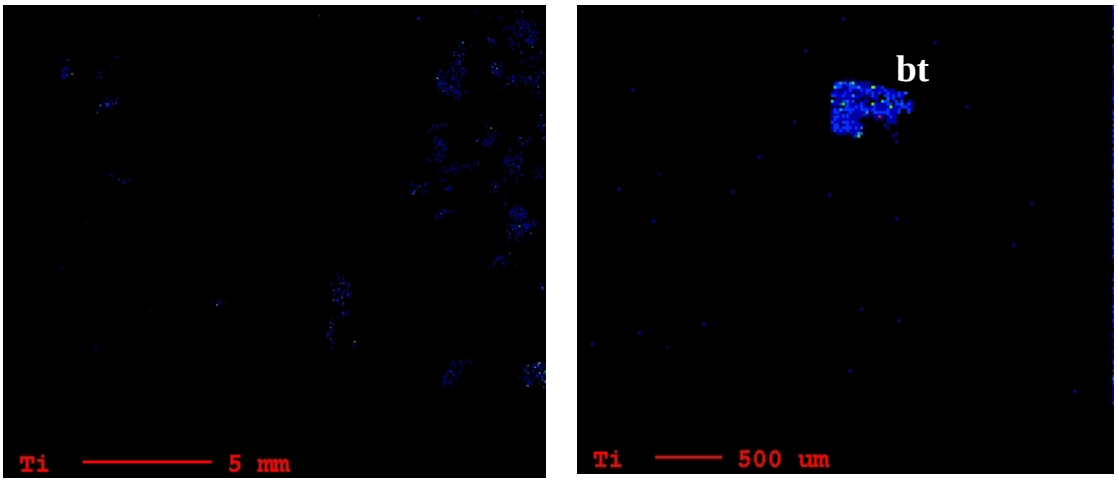

Figure 4.15. A microprobe image, which focuses on the concentrations of Ti. The grains of biotite (bt) have trace amounts of Ti. Accessory minerals found within biotite have higher concentrations of Ti and are observed in the image on the right-hand side.

4.6.2.4 Magnesium

The element Mg shows a concentration in the biotite crystals and the megacryst has trace amounts of Mg (Fig. 4.16).

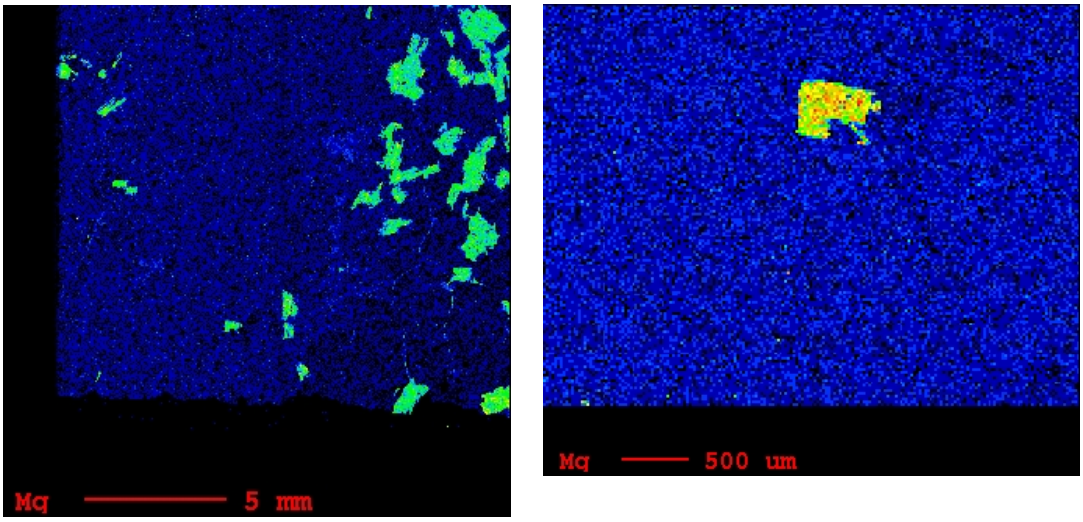

Figure 4.16. An image, which is composed of the concentrations of Mg. The spectral values had to be reduced to observe the trace amounts of Mg.

4.6.2.5 Calcium

Calcium exhibits a weak concentration in plagioclase. There are artifacts of high calcium content (red colour) that are observed to be in the interstitial space near the biotite crystal structure (Fig. 4.17).

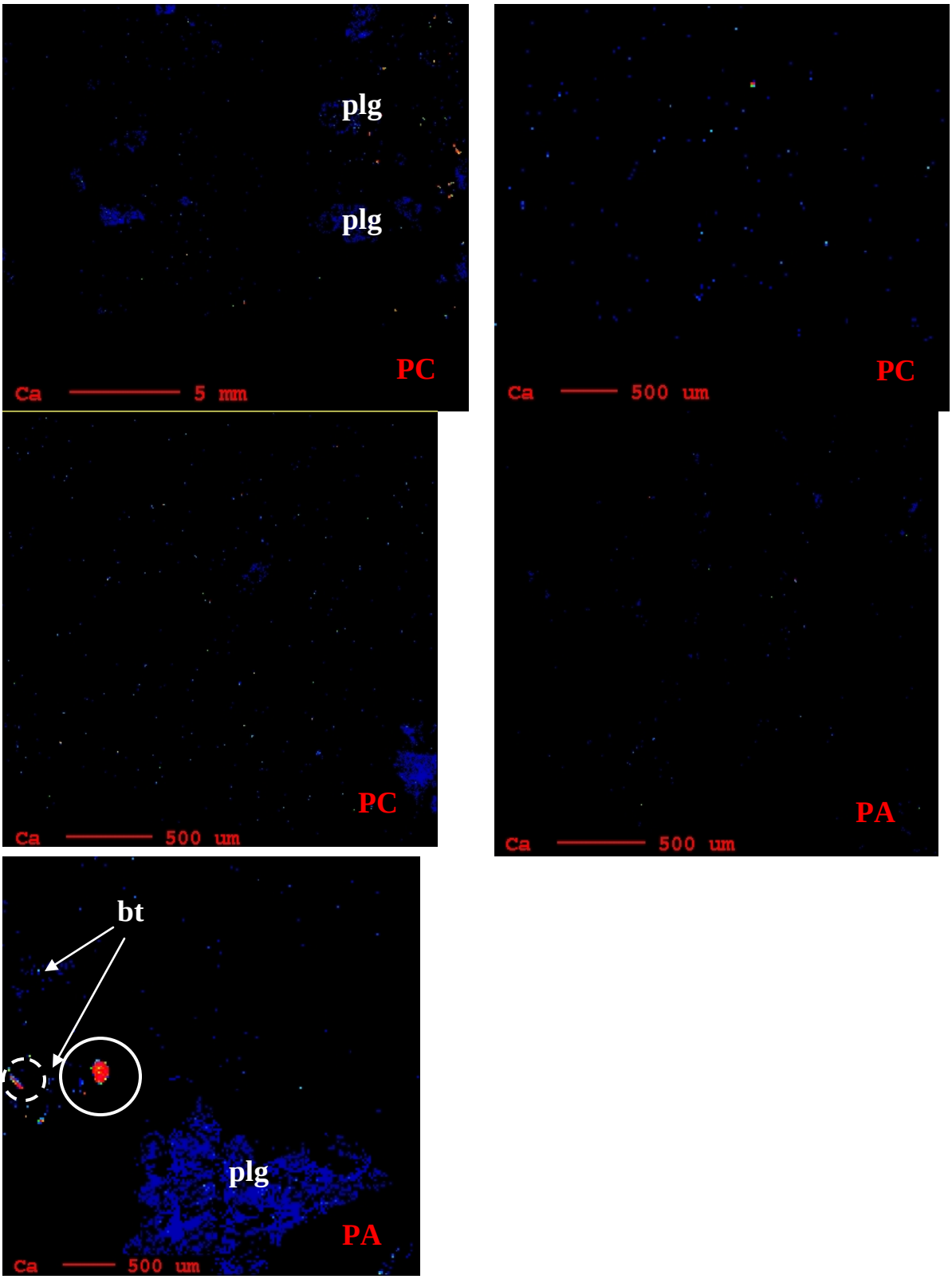

Figure 4.17. A series of five images that show the concentrations of Ca. The Ca is in trace amounts in plagioclase and in large concentrations of apatite on the margins of biotite circled in white.

4.6.2.6 Barium

Barium shows trace amounts within the megacryst, the colour has gradation in intensity from core to rim in repeating sequences. This displays a concentric zoning (Fig.4.10). Barium is also present in low quantities within the biotite; however, it is absent from plagioclase (Fig. 4.18).

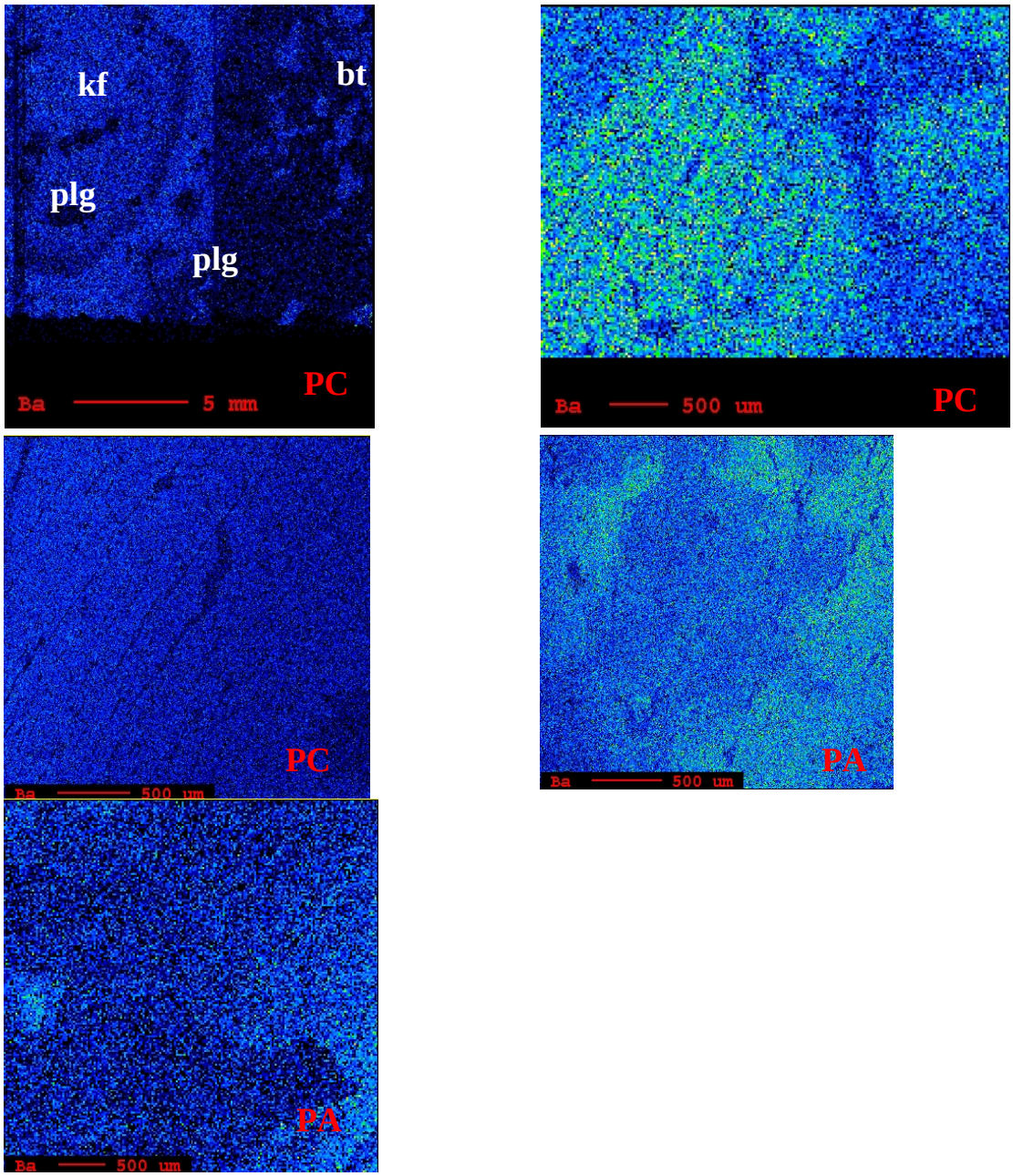

Figure 4.18. Five images that show Ba concentrations. Although, there is gradation in all the frames, the large PC map at the topmost left shows a concentric zoning pattern; whereas, the PA sample shows patchy zoning.

4.6.2.7 Sodium

Sodium concentrations serve to define plagioclase and as might be expected, are also found in perthitic K-feldspar. The plagioclase and perthite show a moderate to high concentration, which is represented by a green and yellow pattern with red highlights toward the margin (Fig. 4.19). The K-feldspar megacryst has a low concentration as registered by the blue colouration (Fig. 4.19).

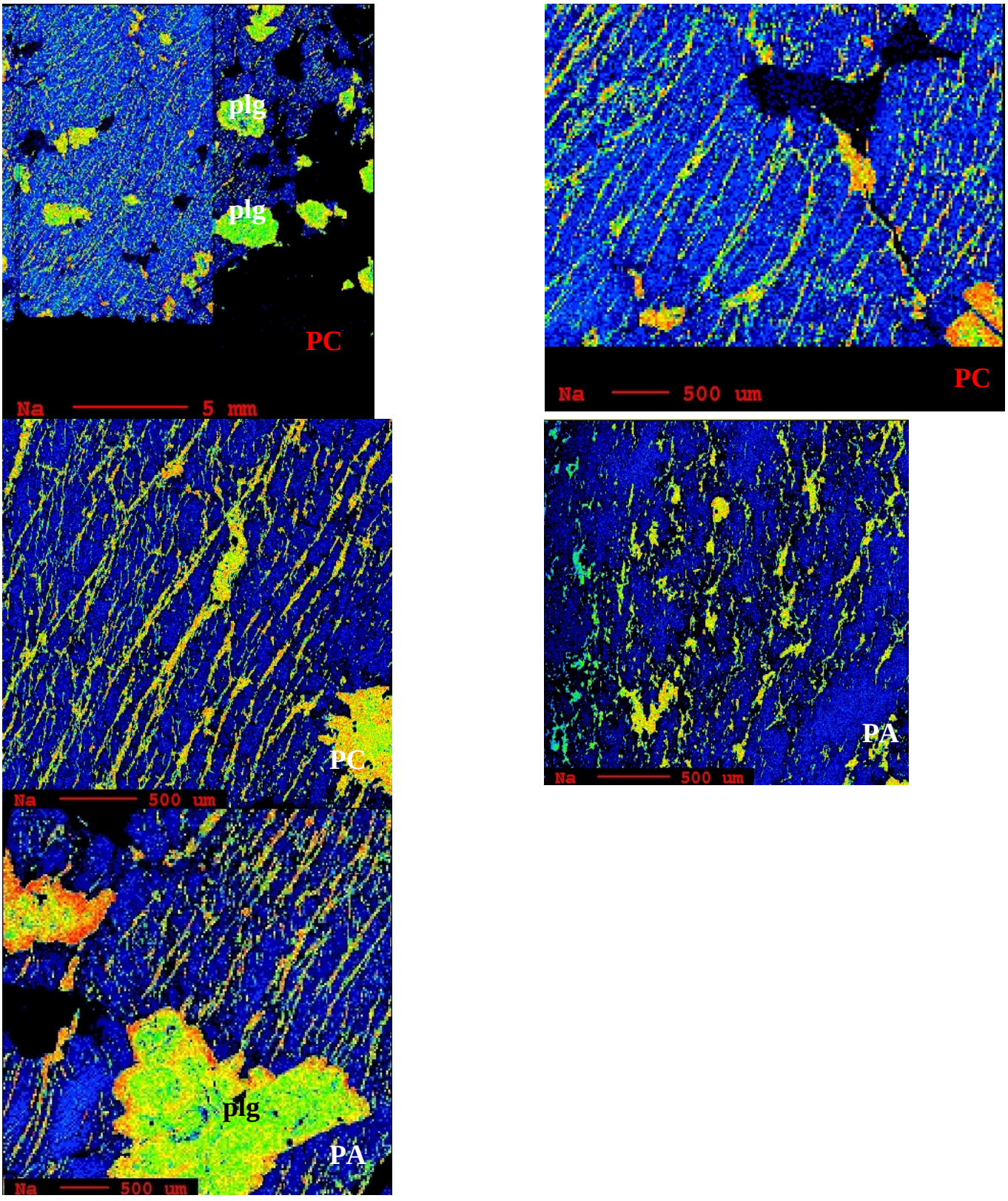

Figure 4.19. A series of probe images, which show Na concentrations primarily in plagioclase, and in perthite. There is observed gradation in the last frame on the margins (more to less) toward the core.

4.6.2.8 Aluminum

Aluminum is observed in the K-feldspar, plagioclase, and biotite. The aluminum concentration in K-feldspar is moderate (green to yellow). The plagioclase is slightly higher in Al than the K-feldspar, and is represented by a yellow colour in Figure 4.20 (PC). Plagioclase also is located in the lower half, right side in a fracture of the K-feldspar crystal (Fig. 4.20). The biotite has a blue-green colour, representing relatively lesser amounts of Al present.

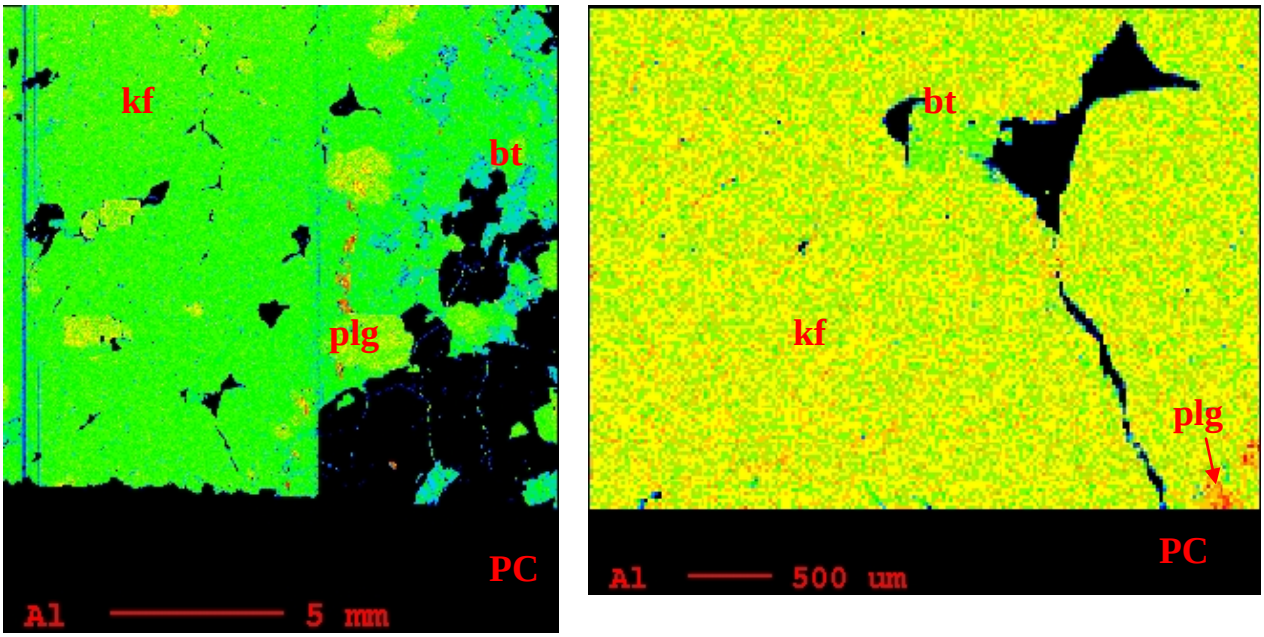

Figure 4.20. Two images that represent the amount of Al within the analyses. There are stronger Al concentrations in feldspars, than in biotite grains. The observation of the megacryst in the right image shows a higher colour value for all minerals.

4.6.2.9 Strontium

The Sr has trace amounts that are obscured in the image. The image looks nearly uniform throughout (Fig. 4.21).

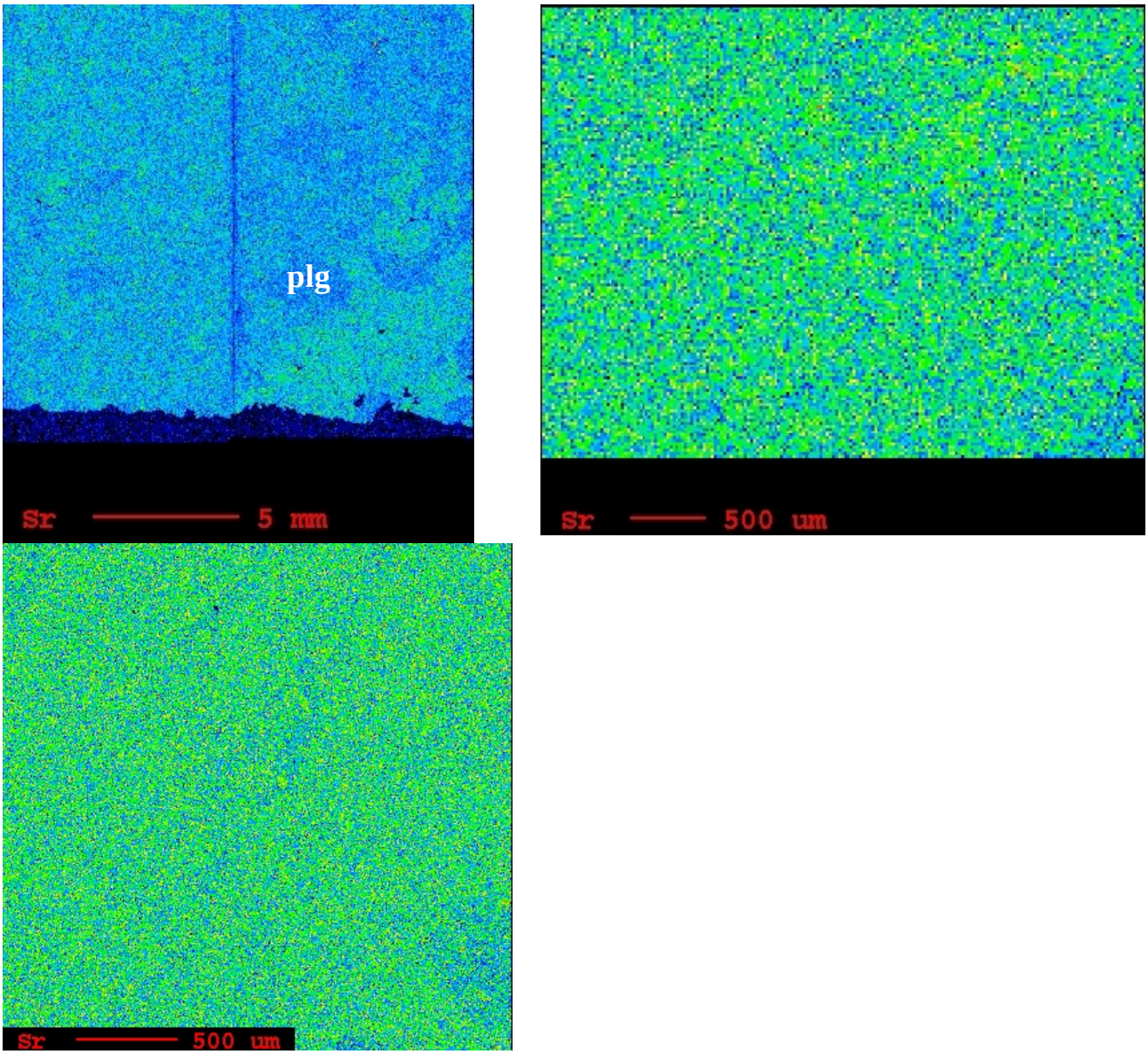

Figure 4.21. Most of the images of Sr concentrations are uniform. The top-left image shows that plagioclase has low to no amount of Sr.

4.6.2.10 Manganese

The Mn shows trace amounts in parts of the biotite crystals and parts of plagioclase, which are represented in dark blue (Fig. 4.22). The fractures in the megacryst have traces of manganese (Fig. 4.22).

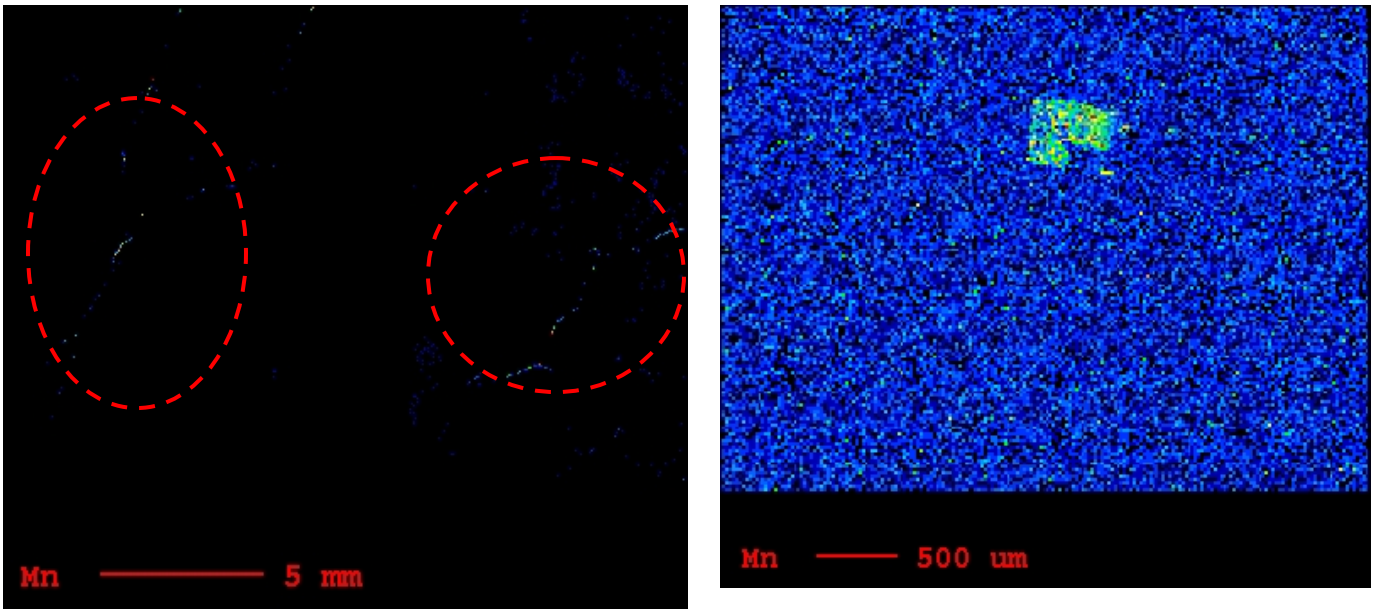

Figure 4.22. The two images, show Mn concentrations are low. The fractures are circled in red. The figure on the left shows a biotite grain with no other minerals present with concentrations of Mn.

4.7 Tables

The microprobe data were used to compose several graphs and data sets. The results of the microprobe show small element concentrations of Cr_2O3, CaO, MnO, TiO, MgO, FeO and Eu_2O_3. Refer to Appendix D for line scan data.

Table 4.1

Microprobe Results in Mass Percent

No	K2O	Cr2O3	Na2O	SiO2	MnO	CaO	TiO2	MgO	Al2O3	FeO	BaO	SrO	Eu2O3	Total	Comment
1	15.28	0	0.972	64.44	0.014	0.011	0	0.012	18.48	0.046	0.091	0.392	0.027	99.76	Line 1 section12line1
2	12.3	0	3.156	64.53	0.003	0.053	0	0	18.44	0.018	0.052	0.38	0.013	98.95	Line 2 section12line1
3	14.87	0	1.232	64.51	0.011	0.03	0.027	0.007	18.36	0.029	0	0.381	0.01	99.46	Line 3 section12line1
4	14.38	0	1.445	64.54	0	0.026	0.007	0.002	18.48	0.011	0.012	0.409	0.006	99.31	Line 4 section12line1
5	15.8	0.002	0.441	64.04	0.012	0.081	0.017	0.013	18.36	0.027	0.022	0.41	0.008	99.23	Line 5 section12line1
6	15.56	0	0.585	63.46	0.011	0.018	0	0.016	18.03	0.033	0	0.377	0.035	98.13	Line 6 section12line1
7	15.64	0.012	0.576	63.42	0.004	0.028	0	0.216	18.32	0.026	0	0.385	0.009	98.64	Line 7 section12line1
8	13.99	0.012	1.674	64.15	0	0.08	0	0.034	19.02	0.036	0.273	0.412	0.005	99.68	Line 8 section12line1
9	15.64	0	0.344	63.65	0	0	0	0.004	18.08	0.028	0.054	0.373	0.017	98.19	Line 9 section12line1
10	15.59	0	0.713	63.73	0	0.05	0	0.013	18.07	0.032	0.15	0.372	0.007	98.72	Line 10 section12line1
11	15.75	0	0.485	63.96	0.002	0	0	0.013	18.3	0.024	0.081	0.374	0.036	99.03	Line 11 section12line1
12	13.69	0	2.456	64.61	0	0.004	0	0.012	18.33	0.008	0.223	0.372	0.017	99.72	Line 12 section12line1
13	15.42	0	0.958	64.53	0.001	0	0.015	0.005	18.43	0.011	0.14	0.396	0.015	99.92	Line 13 section12line1
14	4.223	0.019	0.11	17.73	1.585	41	0	0.101	5.66	0.159	0.033	0.075	0.078	70.77	Line 14 section12line1
15	15.19	0.014	0.655	64.1	0	0	0	0.01	18.24	0.025	0.044	0.378	0.029	98.69	Line 15 section12line1
16	15.06	0	1.191	64.49	0	0.013	0.001	0.016	18.26	0.025	0.084	0.397	0.004	99.54	Line 16 section12line1
17	15.14	0.006	1.103	64.5	0	0.01	0	0.01	18.32	0.018	0.024	0.405	0.055	99.59	Line 17 section12line1
18	15.29	0	0.959	64.34	0.008	0.032	0	0.006	18.32	0.017	0.046	0.389	0.056	99.46	Line 18 section12line1
19	15.92	0.016	0.402	63.82	0.002	0	0	0	18.24	0.034	0.009	0.409	0.036	98.89	Line 19 section12line1
20	0	0	0	98.86	0	0	0	0.004	0	0	0	0.624	0.002	99.49	Line 20 section12line1
21	0.01	0	0	98.93	0	0	0	0.008	0.007	0.006	0	0.639	0	99.6	Line 21 section12line1
22	0.231	0	9.845	64.41	0	3.094	0	0	21.78	0	0	0.313	0.013	99.69	Line 22 section12line1
23	0.168	0	10.16	65.14	0.003	2.28	0	0	21.16	0.007	0	0.31	0	99.23	Line 23 section12line1
24	0.287	0	10.17	65.15	0.009	1.964	0	0	20.93	0	0	0.427	0.003	98.94	Line 24 section12line1
25	13.82	0	1.395	61.21	0	0.023	0.021	0.006	18.17	0.027	0.15	0.377	0.042	95.24	Line 25 section12line1
26	14.96	0	1.249	64.6	0.008	0.029	0	0	18.37	0.028	0.284	0.362	0.034	99.92	Line 26 section12line1
27	14.24	0	1.514	62.85	0	0.021	0.018	0.006	17.88	0.002	0.163	0.338	0	97.04	Line 27 section12line1
28	10.3	0	0.616	43.22	0	0.015	0	0.03	16.02	0.021	0.232	0.211	0	70.66	Line 28 section12line1

4.8 Two-feldspar Geothermometry

The two-feldspar geothermometer results reveal two separate ranges of temperature for the Peggy's Cove and Prospect Area. The results exhibit a higher temperature range for megacryst crystallization in PC than in PA. The temperature of crystallization for megacrysts in Peggy's Cove range from a high of 981^{o}C using geotherms of Elkins & Grove (1990) to a possible low of 775^{o}C as given by Putirka (2008). The three components of a tri-plot: anorthite (AN), the Ca-rich end-member of feldspar; albite (AB), the Na-rich end-member; K-feldspar or orthoclase (OR), the K-rich end-member exhibit different concentrations depending on position between the core to the rim (Figs. 4.23 & 4.25). The referred 'whole rock' in the diagrams and whole crystal in this section is the non-segregated feldspar composition of perthite and K-feldspar.

4.8.1 Peggy's Cove

In Table 4.2, the K-feldspar exhibits low amounts of albite (~10%) and lesser amounts of anorthite (< 0.5%). The perthite is comprised of mostly albite. The whole crystal (K-feldspar and perthite) composition is about 27% albite, ~2% anorthite and ~71% orthoclase (K-feldspar). Within the plagioclase inclusion albite contents vary from An_{26} in the core, to An_{37} towards the rim, with values between An_{23-25} in the outermost rim (Table 4.2).

Table 4.2

Results of the Peggy's Cove Two-feldspar Geothermometer

Trial		Max	Min	core	Exsolution	exsl max	exsl min	max	min
K1		906.2627	788.1932			519.6189	483.0011	906.2627	788.1932
L1		906.2627	788.1932			519.6189	483.0011	981.6092	844.1968
Q1		906.2627	788.1932			519.6189	483.0011	980.0323	843.0342
						519.6189	483.0011	894.5866	780.8185
	2	981.6092	844.1968			519.6189	483.0011	887.9897	775.802
		981.6092	844.1968						
		981.6092	844.1968						
	3	980.0323	843.0342						
		980.0323	843.0342						
		980.0323	843.0342						
	4	894.5866	780.8185						
		894.5866	780.8185						
		894.5866	780.8185						
	5	887.9897	775.802						
		887.9897	775.802						
		887.9897	775.802	rim					

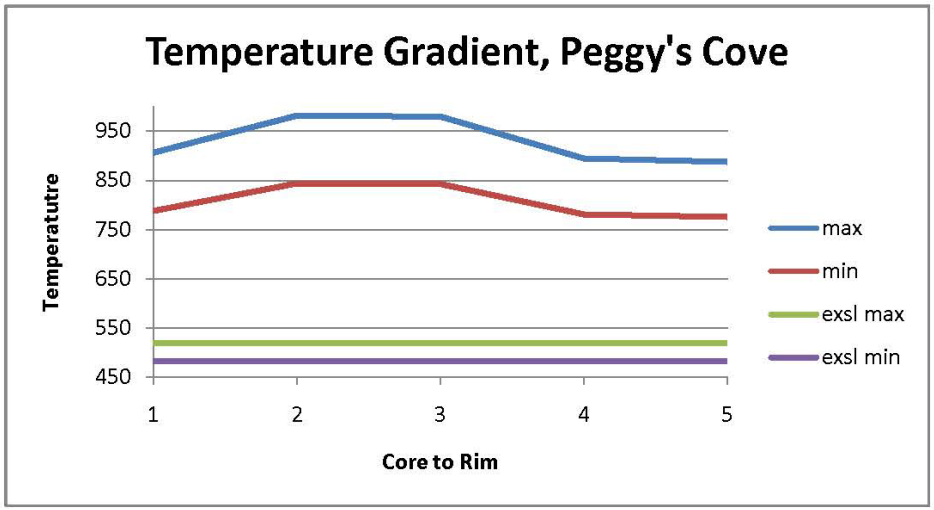

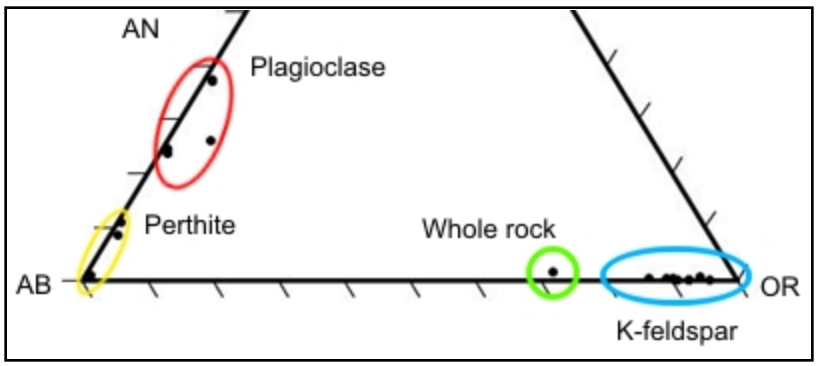

Figure 4.23. A tri-plot of Peggy's Cove end-member data. The plot is cut at the level, AN 50%; the partition was created since no data passed this point. Potassium feldspar is circled in blue; whole rock is in green; perthite in yellow, and plagioclase in red.

Temperatures recorded from the Peggy's Cove sample show a range from an average maximum temperature of 913^{o}C to 832^{o}C using the variation in compositions across a zoned plagioclase inclusion (Figure 4.25). The slope of the temperature gradient is low suggesting that the variation in temperatures during the growth of the megacryst cores was small. The average temperature for the exsolution of perthite from K-feldspar based on recalculated compositions is 502^{o}C.

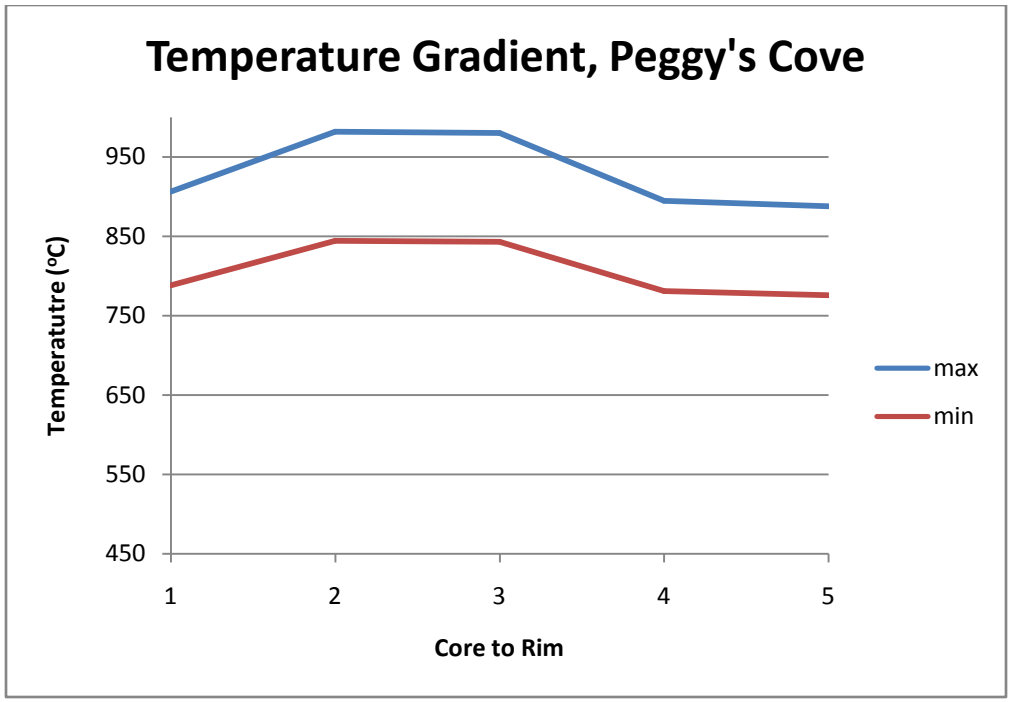

Figure 4.24. A graph expressing isotherms of Peggy's Cove, derived by equations of Elkins and Grove (1990) as given in Putirka (2008).

4.8.2 Prospect Area

The data for Prospect area displays less anorthite content than Peggy's Cove. The occurrence of exsolution lamellae happens at a temperature range from 530°C to 586°C (Table 4.3), which is a little higher than the Peggy's Cove data.

Table 4.3

Results for Prospect Area From Two-feldspar Geothermometer

Trail		max	min	exsl max	exsl min	max	min
K1		837.8808	709.9022	586.3331	529.8343	837.8808	709.9022
L1		837.8808	709.9022	586.3331	529.8343	842.3864	713.0896
Q1		837.8808	709.9022	586.3331	529.8343	772.1813	662.3772
				586.3331	529.8343	755.0725	649.7792
	2	842.3864	713.0896	586.3331	529.8343	722.6972	625.5965
		842.3864	713.0896				
		842.3864	713.0896				
	3	772.1813	662.3772				
		772.1813	662.3772				
		772.1813	662.3772				
	4	755.0725	649.7792				
		755.0725	649.7792				
		755.0725	649.7792				
	5	722.6972	625.5965				
		722.6972	625.5965				
		722.6972	625.5965				

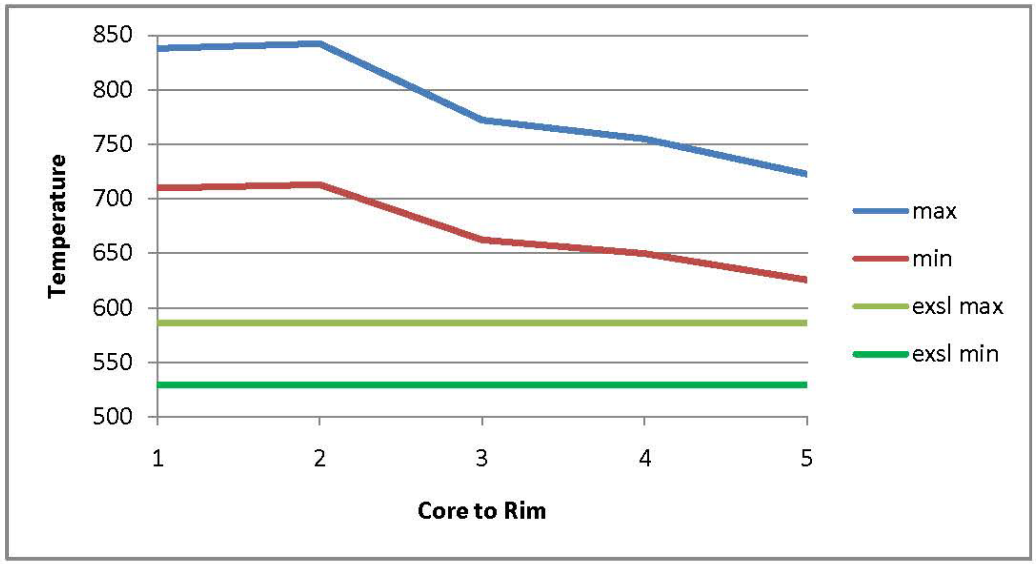

The end-member data of Prospect shows K-feldspar and the whole rock, both with albite concentrations lower than thirty percent (Fig. 4.25). Plagioclase and perthite have similar values in anorthite and albite (Fig. 4.25). The outlier in Figure 4.25 was observed in the perthite calculations.

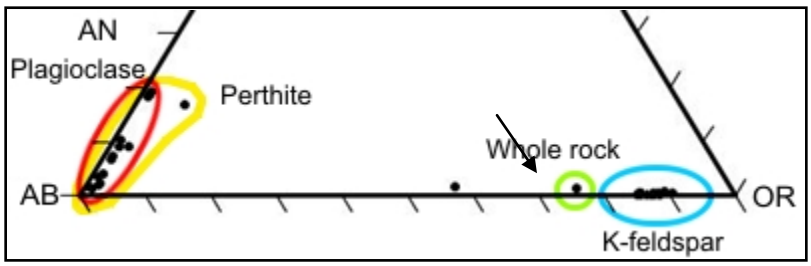

Figure 4.25. A tri-plot that displays groups of feldspar phases found within the K-feldspar megacryst. The outlier is marked by an arrow.

The overall character of the temperature trend of the Prospect area is a decreasing gradient from core to rim (Fig. 4. 26). This is in contrast to the temperature fluctuations observed for PC (Fig. 4.24). The average temperature in the core has a value of 774 - 778^{o}C, and moving outwards, the overall pattern is one of decreasing temperature from core to rim, with a near-rim temp estimate of 717^{o}C.

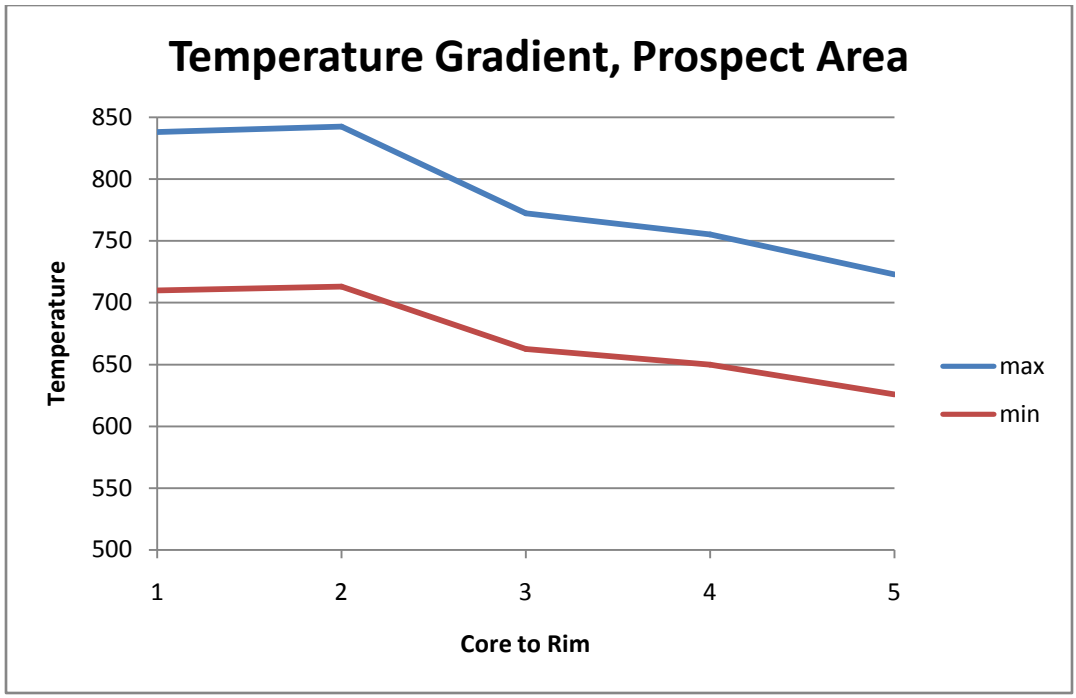

Figure 4.26. Temperature ranges for K-feldspar plagioclase inclusions in the Prospect area.

Chapter 5: Discussion

5.1 Introduction

Clarke and Clarke (1998) concluded that the K-feldspar megacrysts formed in magmatic conditions, under a range of pressure, temperature, and composition within the South Mountain Batholith. Also, Long and Luth (1986) and Cox et al. (1996) working on granites elsewhere, concluded that fluctuating levels of Ba in traversing, from core to rim within a K-feldspar megacryst exhibit concentrations that indicate magma-mixing. The heterogenetic nature of the South Mountain Batholith, as evidenced by the variability of the rock within a single pluton and the nature of the textures such as oscillatory zoning within the rock, suggest that determining the relative timing of K-feldspar crystal growth is difficult to establish firmly. A number of possible explanations have been proposed for such heterogeneity in granitoid rocks: crustal contamination; magma mixing; instability; and volatile interaction (Cox et al., 1996). These factors are the controllers that influence structures, textures and subsolidus changes in granitoids (Cox et al., 1996). This study aims to test the hypothesis that magma mixing is an important contributor to the heterogeneity within the SMB. In order to test this hypothesis, megacrysts from the biotite monzogranite were analysed in particular, in order to determine the nature of Ba distribution within the megacrysts, as Ba distribution has been shown to be linked to magma mixing (ex. Cox et al. 1996). Prospect area mineral textures suggest that there was little to no metamorphism by magmatic injection in the stages after the initial crystallization of K-feldspar megacrysts. The textural and mineralogical evidence is consistent with differentiation as predicted by Bowen's Reaction Series.

This chapter discusses the evidence for magma mixing from a detailed study of K-feldspar megacrysts in two variants of the same Halifax Pluton of the South Mountain Batholith.

5.2 Evidence for Magma Mixing: Field Observations and Petrography

There are a number of features observed in the field that support magma mixing. The presence of autoliths in the granite and the presence of mantling by plagioclase of K-feldspar megacrysts. In addition, the megacrysts display both internal zoning and subhedral morphology, which suggests periods of resorption.

Whereas a number of K-feldspar megacrysts are large, euhedral crystals (4 x1.5 cm), others are typically smaller, rounded (1-04a), subhedral, and difficult to recognize from other phases such as plagioclase. Exsolution lamellae can be seen on the faces of the megacrysts but whether it is perthite or antiperthite cannot be distinguished with the naked eye. In summary, the presence of autoliths, internal zoning and a variation from euhedral to subhedral megacrysts strongly suggests a reabsorbing and/or reheating event in these segments of the Halifax Pluton.

Plagioclase is massive, subhedral to euhedral and displays polysynthetic twinning in the groundmass. Plagioclase inclusions within the K-feldspar megacrysts display identical textures. Oscillatory zoning is common within the plagioclase crystals. Oscillatory zoning is commonly interpreted to be the result of either a) repeated phases of growth in equilibrium with the local melt (Slaby & Gotze, 2004), or b) reheating and resorption as a result of magma mixing (Moore & Sisson, 2008). Within the plagioclase studies narrow zones are interpreted to most likely represent repeated phases of equilibrium growth and the wider zones suggests partial resorption of the crystal. These textures are observed in thin section (Fig. 4. 7 B) and using cathodoluminescence (Fig. 4. 8). The composition of the plagioclase inclusions range from $An_{26\text{-}18}$ in the core to $An_{24\text{-}0.5}$ in the rim. This variation in An content along with the fine scale and large scale oscillatory zoning suggests that both equilibrium growth (Ca fractionation) and resorption have both occurred during the crystallization of the plagioclase.

Plagioclase crystals contain greater amounts of Ca in the PC samples versus the PA samples. This suggests that the samples at PC grew from a slightly more mafic magma than those of PA and this interpretation is consistent with the continuous crystallization sequence in Bowen's Reaction Series (Fig. 5.1)

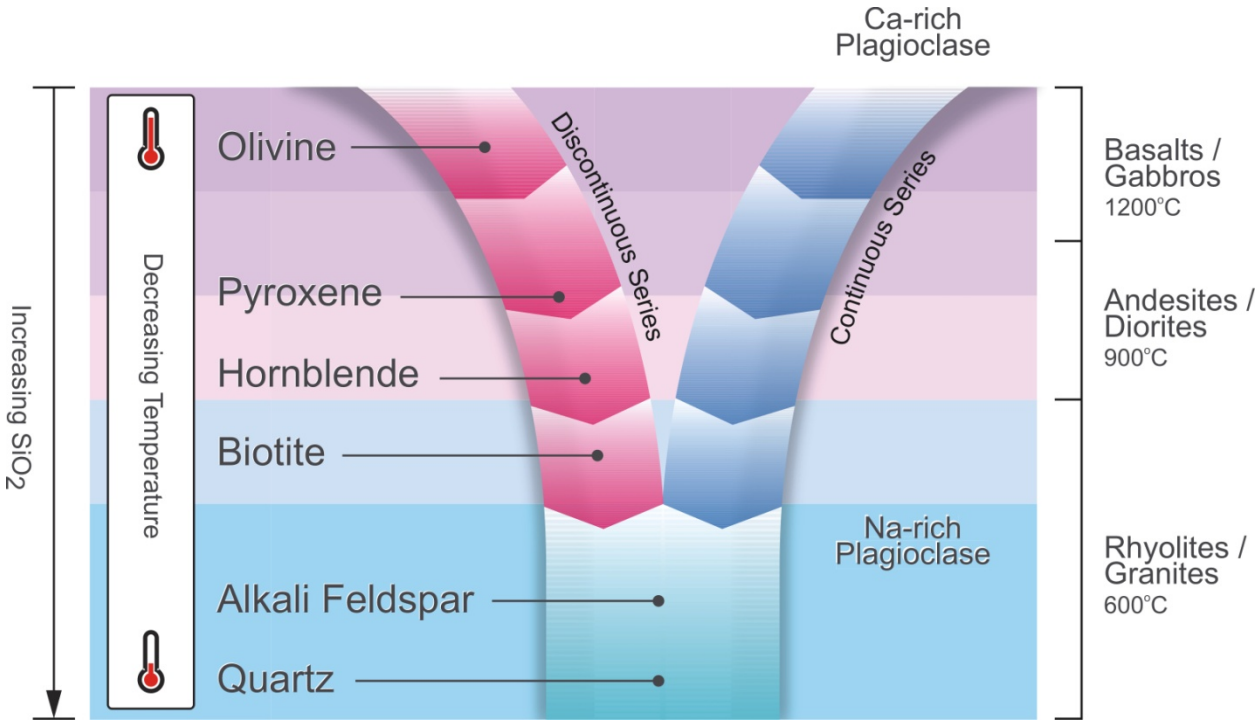

Figure 5.1. A diagram after Bowen's Reaction Series that show trends (SiO2 concentrations, temperature and temp. boundaries) of common rock building minerals.

5.3 Evidence for Magma Mixing: Cathodoluminescence

Under cathodoluminescence the K-feldspar megacrysts from the PC samples show patchy zonation and randomly distributed plagioclase inclusions (Fig 4.8). In contrast, the K-feldspar megacrysts from PA show regular growth zoning with aligned plagioclase inclusions (Fig. 4.10). The variation in these textures can be explained as follows: the megacrysts from PC have undergone significant resorption and regrowth. The megacrysts from PA on the other hand

appear to have crystallized in a steady state manner in the cooling granitic magma. Other examples of oscillatory zoning observed by Cox et al. (1996) indicates that minor and trace element substitution of the major elements are common in zoned megacrysts, formed in a melt. The colour emitted is determined by the amount of certain trace element activators (eg. blue (460 nm) for Ti^{4+}; red (700 nm) for Fe^{3+}; green (550-570 nm) for Fe^{2+} and Mn^{2+}) and structural defects (Ginibre, Worner, & Kronz, 2004). In the feldspars examined in this study, the zoning patterns, although not as strongly defined as previous studies (eg. Cox et al., 1996) are consistent with these earlier examples. In other words fluctuations in magma input and mixing are recorded by the colour variations in the CL images of this study.

5.4 Evidence for Magma Mixing: Microprobe Analyses

5.4.1 Megacryst microtransects for Ba composition

X-ray mapping of the megacrysts showed that despite the fact that the megacrysts from PC show much less overall variation in Ba contents the distribution of Ba has been influenced by a process of resorption and regrowth. This is evidenced by the formation of a Ba enriched annulus within the megacryst from PC (Fig. 4.18). The fluctuations in BaO from core to rim as shown in the line scan (Fig. 4.11) suggest resorption and regrowth along with variations in temperature (Mehnert & Busch, 1981). This further supports the possibility of the influx of a second magma. This interpretation is similar to the findings of Long and Luth (1986) for the K-feldspar megacrysts in the Peñasco Quartz Monzonite, New Mexico.

Barium distribution in the crystal also indicates variations in concentration from the core to the margin (Fig. 4.11). From the core to the margin the Ba shows an overall decrease. Barium is an incompatible element that prefers to remain in the melt than to precipitate into the crystals.

Upon reheating, barium is one element that is first to proceed into the melt. Nelson (2003) explains upon reaching melting temperatures, a percentage of a mineral will convert from solid to liquid phase, and Ba will be more concentrated in this liquid phase. Subsequently the second zone in the megacryst will form with less of the incompatible element at the beginning of the crystallization process and the incompatible element (Ba) will be more highly concentrated in the edge of this second zone (Nelson, 2003). In addition, if there has been contamination of the magma by Ba-rich crustal rocks during K-feldspar crystal formation, oscillatory zoning would not result. Rather, the result would be higher Ba concentrations of all the minerals formed in the pluton, which would buffer the Ba concentrations resulting in less or no barium zoning in the K-feldspar.

5.5 Evidence for Crystallization and Cooling Histories: Two-feldspar Geothermometer

Mehnert and Busch (1981) observed increasing concentrations of Ba due to increases in temperature during K-feldspar crystallization. The equilibration temperature in Peggy's Cove was calculated to range from 981^{o}C to 775^{o}C, as measured using two-feldspar geothermometry. This temperature range implies that the variation in Ba concentrations and zoning observed, occurred at temperatures >775^{o}C. In addition, the process which produced the variation in Ba must also have occurred between the temperatures between 981^{o}C to 775^{o}C.

In Peggy's Cove, the crystal cooled by approximately 300^{o}C before exsolution occurred. The temperature of exsolution was between 483^{o}C and 520^{o}C (Fig. 4.28). In summary, the megacrysts from PC have undergone resorption and regrowth at temperatures in excess of 775^{o}C. The simplest explanation for the textures and these temperature ranges is high temperature resorption caused by a magma mixing event.

In the Prospect area, there is little evidence of interrupted growth of the K-feldspar megacrysts, and the temperature range (842^{o}C - 625^{o}C) shows a more gradual decrease from core to rim. In addition, the maximum recorded temperature is considerably lower than at Peggy's Cove. As a result of the un-interrupted magmatic growth at PA, oscillatory zoning is found within the megacrysts and both the plagioclase inclusions and matrix crystals (Fig 4.8). Furthermore, there is no evidence from Ba zoning for periods of significant crystal resorption.

The temperature range for exsolution at PA (530^{o}C - 586^{o}C) is higher than at PC (483^{o}C - 520^{o}C). This can be explained by the fact that the megacrysts from PC have undergone high temperature resorption, which resulted in Ca depletion prior to exsolution. The megacrysts at PA did not experience this high temperature resorption event and thus retained higher Ca content than those at PC. This in turn caused perthite exsolution to occur at a higher temperature at PA.

Although the evidence points to the possibility of an injection of a second magma, it could be argued that the thermal gradient suggested by the variation in temperatures recorded by the megacrysts from Peggy's Cove to Prospect was caused by interaction with the cool country rock. However, this does not explain the apparent increase in temperatures or spikes in Ba concentrations in the Peggy's Cove megacrysts.

If the spikes in Ba concentrations within the megacrysts were caused by country rock contamination, the concentration of Ba would show an increase from core to rim in the megacrysts. At PC, the overall variation in Ba concentrations in the megacrysts is small and indeed, the variation which does exist suggests the opposite trend, e.g. a reduction in Ba concentrations from core to rim.

Chapter 6: Conclusion

The textures and chemical zoning patterns recorded by the K-feldspar megacrysts and cogenetic plagioclase crystals in the samples examined in this study indicate an igneous origin. However, the two sample areas record somewhat different magmatic histories. For example, the megacrysts from Peggy's Cove show evidence for resorption and variations of in Ba, which suggest the partial dissolution and regrowth at high temperatures. The megacrysts from Prospect area are more abundant, euhedral and contain inclusions of plagioclase with oscillatory zoning, which were trapped by the growing megacrysts and became aligned against the crystal faces. These megacrysts also show less evidence of Ba zoning and resorption.

In terms of temperature variations recorded by the megacrysts, two-feldspar geothermometry suggests the maximum recorded crystallization temperatures of 981^{o}C for the Peggy's Cove megacrysts and 842^{o}C for those from Prospect. In addition, the temperatures for exsolution are also different with the megacrysts at Peggy's Cove recording a maximum temperature of 520^{o}C, whereas the megacrysts at Prospect record a maximum temperature of exsolution of 586^{o}C. This is likely to be due to the loss of Ca during resorption of the megacrysts at high temperatures in the samples from Peggy's Cove, which did not occur in the samples from Prospect.

The most likely explanation for the textures, differences in chemical zonation and recorded temperatures and the variations between the samples from Peggy's Cove and Prospect, is that a high temperature event occurred during emplacement of this section of the Halifax Pluton. The most plausible explanation for this event is magma mixing, ie an injection of higher

temperature magma(s) into the crystallizing Halifax Pluton. This magma mixing event affected the megacrysts at Peggy's Cove, but had less of an effect on the megacrysts at Prospect.

References

Browne, B. L., Eichelberger, J. C., Patino, L. C., Vogel, T. A., Uto, K., & Hoshizumi, H. (2006). Magma mingling as indicated by texture and Sr /Ba ratios of plagioclase phenocrysts from Unzen volcano, SW Japan. *Journal of Volcanology and Geothermal Research* (154), 103-116.

Clarke, D. B., & Clarke, G. K. (1998). Layered granodiorites at Chebucto Head, South Mountain batholith, Nova Scotia. *Journal of Structural Geology , 20* (9), 1305-1324.

Cox, R. A., Dempster, T. J., Bell, B. R., & Rogers, G. (1996). Crystallization of the Shap Granite: evidence from zoned K-feldspar megacrysts. *Journal of the Geological Society , 153,* 625-635.

Elkins, L. T., & Grove, T. L. (1990). Ternary feldspar experiments and thermodynamic models. *American Mineralogist , 75*, 544-559.

Freda, C., & Baker, D. R. (1998). Na-K interdiffusion in alkali feldspar melts. *Geochimica et Cosmochimica Acta , 62* (17), 2997-3007.

Friel, J. J. (1995). *X-ray and Image Analysis in Electron Microscopy.* New Jersey: Princeton Gamma-Tech.

Gagnevin, D., Daly, J. S., Waight, T. E., Morgan, D., & Poli, G. (2004). Pb isotopic zoning of K-feldspar megacrysts determined by Laser Ablation Multi-Collector ICP-MS: Insights into granite petrogenesis. *Geochimica et Cosmochimica Acta , 69* (7), 1899-1915.

Graham, D. J., & Midgley, N. G. (2003). *Tri-plot: Ternary diagram plotting software*. Retrieved January 19, 2013, from Loughborough University Department of Geology: http://www.lboro.ac.uk/research/phys-geog/tri-plot/index.html

Hacettepe University Department of Mining Engineering. (2013). *Dictionary of Mining, Mineral, and Related Terms*. Retrieved December 13, 2012, from Hacettepe University Department of Mining Engineering: http://www.maden.hacettepe.edu.tr/dmmrt/

Harlov, D. E., Hansen, E. C., & Bigler, C. (1998). Petrologic evidence for K-feldspar metasomatism in granulite facies rocks. *Chemical Geology , 151* (1–4), 373-386.

Imtiaz, H. (2007). Petrogenesis of Enclaves Within the Peggy's Cove Monzogranite, Southern Nova Scotia, Canada. *20th Annual Keck Symposium* (pp. 255-261). Trinity University.

Insights into granite petrogenesis from quantitative assessment of the field distribution of enclaves, xenoliths and K-feldspar megacrysts in the Monte Capanne pluton, Italy2008*Mineralogical Magazine 72*4925-940

JEOL. (2012). *JXA-8230 SuperProbe Electron Probe Microanalyzer (EPMA)*. Retrieved February 2, 2013, from JEOL: Global Solutions Provider for Advanced Technology: http://www.jeol.com/

Johnson, B. R., & Glazner, A. F. (2010). Formation of K-feldspar megacrysts in granodioritic plutons by thermal cycling and late-stage textural coarsening. *Contrib Mineral Petrol , 159*, 599–619.

Long, P. E., & Luth, W. C. (1986). Origin of K-feldspar megacrysts in granitic rocks: Implications of a partitioning model for barium. *American Mineralogist , 71*, 367-375.

MacDonald, M. A. (2001). *Geology of the South Mountain Batholith, Southwestern Nova Scotia.* Halifax: Nova Scotia Natural Resources.

MacDonald, M. A., Horne, R. J., Corey, M. C., & Ham, L. J. (1992). An overview of recent bedrock mapping and follow-up petrological studies of the South Mountain Batholith, southwestern Nova Scotia, Canada. *Atlantic Geology* (28), 7-28.

McCuish, K. L. (2001). *Schieren in the South Mountain Batholith and Port Mouton Pluton Meguma Zone, Nova Scotia.*

McLemore, V. T., & Barker, J. M. (1987). Some geological applications of cathodoluminescence. *New Mexico Geology* , 37-40.

Mehnert, K. R., & Busch, W. (1981). The Ba content of K-feldspar megacrysts in granites: a criterion for their formation. *N. Jb. Min. Abh. , 140*, 221-252.

Merriam-Webster Incorporate2013*An Encyclopaedia Brittanica Company: Merriam-Webster*

Moore, J. G., & Sisson, T. W. (2008). Igneous phenocrystic origin of K-feldspar megacrysts in granitic rocks from the Sierra Nevada batholith. *Geosphere , 4* (2), 387-400.

Nelson, S. A. (2003, November 7). *Magmatic Differentiation*. Retrieved February 17, 2013, from Tulane Universitiy: http://www.tulane.edu/~sanelson/eens211/magmadiff.htm

Nesse, W. D. (2000). *Introduction to Mineralogy.* New York: Oxford University Press.

Nova Scotia Department of Natural Resources. (1994). *Geological Map of the South Mountain Batholith: Western Nova Scotia.* Halifax: Nova Scotia Department of Natural Resources.

Orville, P. M. (1963). Alkali ion exchange between vapor and feldspar phases. *American Journal of Science , 261*, 201-237.

Province of Nova Scotia. (2013, March 7). *DNR Library*. Retrieved March 10, 2013, from Nova Scotia Department of Natural Resources: https://www.gov.ns.ca/natr

Pupier, E., Barbey, P., Toplis, M. J., & Bussy, F. (2008). Igneous Layering, Fractional Crystallization and Growth of Granitic Plutons: the Dolbel Batholith in SW Niger. *Journal of Petrology , 49* (6), 1043-1068.

Putirka, K. D. (2008). Thermometers and Barometers for Volcanic Systems. *Reviews in Mineralogy & Geochemistry , 69*, 61-120.

Slaby, E., & Gotze, J. (2004). Feldspar crystallization under magma-mixing conditions shown by cathodoluminescence and geochemical modelling - a case study from the Karkonosze pluton (SW Poland). *Mineralogical Magazine , 68* (4), 561-577.

Smith, J. V., & Brown, W. L. (1988). *Feldspar Minerals* (2nd ed., Vol. I). New York: Springer-Verlag.

Stormer, J. C. (1975). A Practical Two-feldspar Geothermometer. *American Mineralogist , 60*, 667-674.

Structure and Dynamics of the Laacher See Magma Chamber (Eifel, Germany) from Major and Trace Element Zoning in Sanidine: a Cathodoluminescence and Electron Microprobe Study2004*Journal of Petrology 45*112197-2223

US Geological Survey. (2012, May 2). Retrieved February 12, 2013, from USGS site: http://www.usgs.gov/

Vernon, R. H., & Paterson, S. R. (2008). How late are K-feldspar megacrysts in granites? *Lithos , 104* (1-4), 327-336.

Winter, J. D. (2010). *An Introduction to Igneous and Metamorprhic Petrology* (2nd ed.). New Jersey: Prentice Hall.

Appendix A

Glossary

phaneritic readily visible crystals (>0.1 mm) that compose the majority of the rock. This texture typically represents slow cooling at depth, below the surface. Two size boundaries for this type of texture are medium grained (**1-5 mm**) and coarse grained that has a range of **5-50 mm**(Winter, 2010).

phenocrysts larger crystals in a finer grained groundmass. Intrusive and extrusive rocks are classified by the grain size of the groundmass (Winter, 2010).

Bowen's Series a group of eight common minerals found in nearly all igneous rocks; those minerals are quartz, plagioclase, alkali feldspar, muscovite, biotite, hornblende, pyroxene and olivine (Winter, 2010).

nucleation the initial step in crystal growth, where the surface area is greater than its volume, which causes surface ions to attract surrounding compatible ions to form a stable lattice (Winter, 2010).

primary twinning is an intergrowth that happens during crystallization from a melt, where there are two crystal orientations (Winter, 2010).

perthite is albite lamellae within a K-feldspar host (Winter, 2010).

exsolution the un-mixing of constituents within a solid solution. A common occurrence is the segregation of Na from K in alkali feldspar (Winter, 2010).

myrmekite is a secondary reaction that occurs during the cooling of granites. It often occurs between the boundary of K-feldspar and plagioclase (Smith & Brown, 1988).

megacrysts are unusually large crystals (Winter, 2010).

typomorphic is the event at which an effect is the result of a particular temperature and pressure (Merriam-Webster, 2013).

diffusivity *is the relative rate of flow per unit area of a particular constituent of a mixture divided by the gradient of composition, temperature, or other property considered to be causing the diffusion* (HUDME, 2013).

Appendix B

Operation of ImageJ

1. Start ImageJ
2. Go to File tab, choose Open and select image file.
3. Choose Straight line button shown here (A), then draw a line from a known reference line (B).

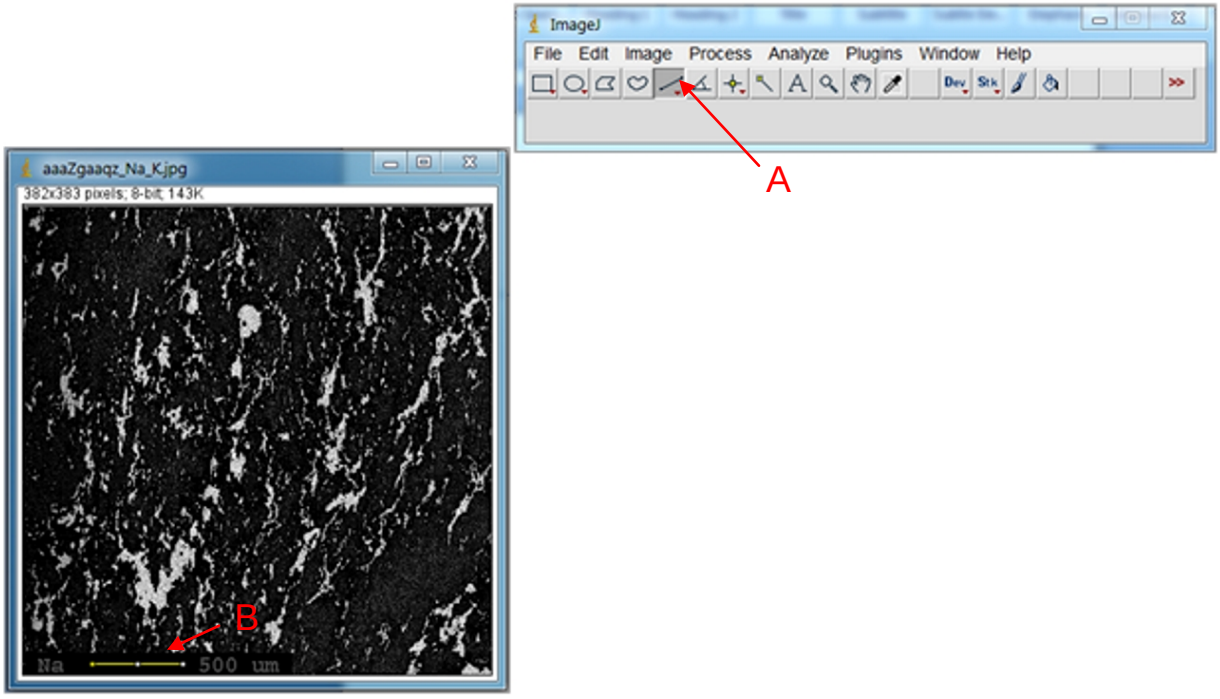

4. Go to the Analyze tab, choose Set Scale.

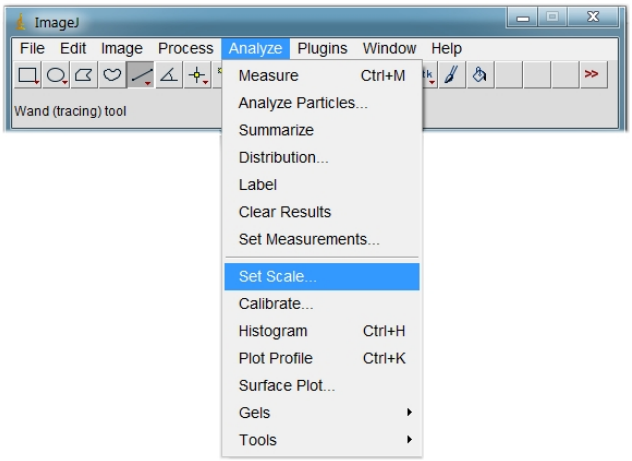

5. In the Set Scale window, change the Known distance to 500 µm, then change the Unit of length to microns and press OK.

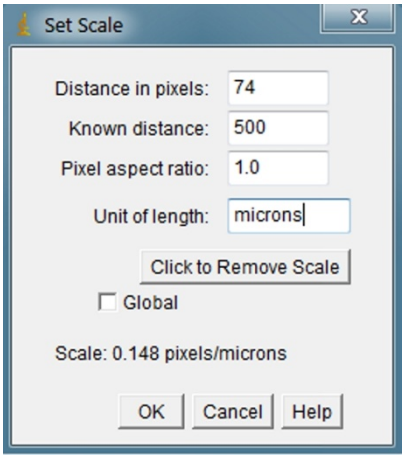

The result is a change in resolution from units to microns, which is located in the upper left margin.

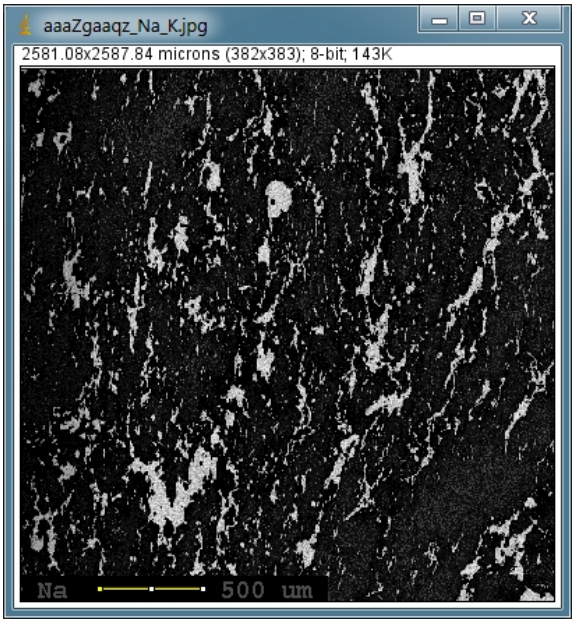

The next step is to isolate the sample area.

6. Now choose the Freehand or Rectangular tool, the buttons located to the left of the Straight line tool. Press and hold left click button, draw a area around the pixels that should be excluded from the results.

7. In the Edit tab, choose clear (white) or fill (black) depending on the hue of the area to be calculated.
8. From the Image tab select Adjust from the drop-down menu and then choose Threshold.
9. In the Threshold window, manipulate the scroll buttons to increase and decrease the white and black boundaries, (to invert the colour of the background, check the Dark Background box) then press apply.

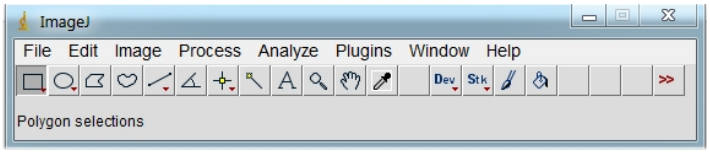

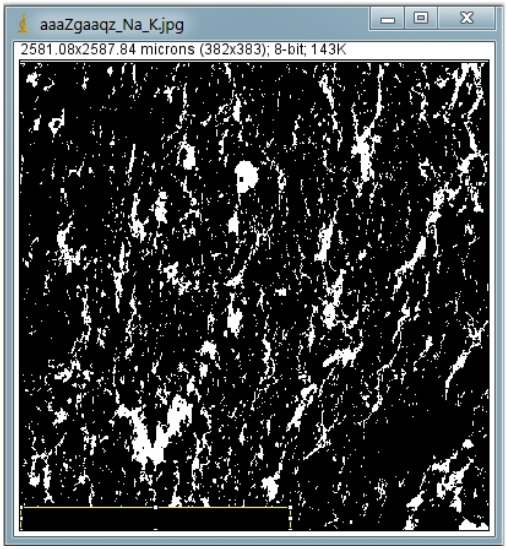

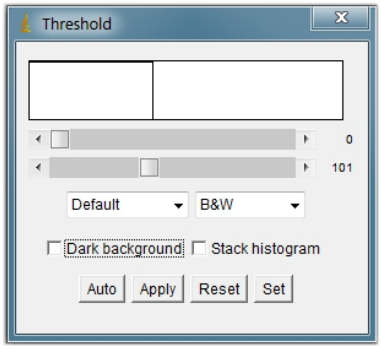

10. Choose the Process tab, cycle down and choose Binary, then Make Binary (this method is used to create two values for more precise calculation). The resulting image looks similar to threshold.

11. Go to the Analyze tab, choose Analyze Particles a window will open. In the Analyze Particle window press Apply for the default settings.

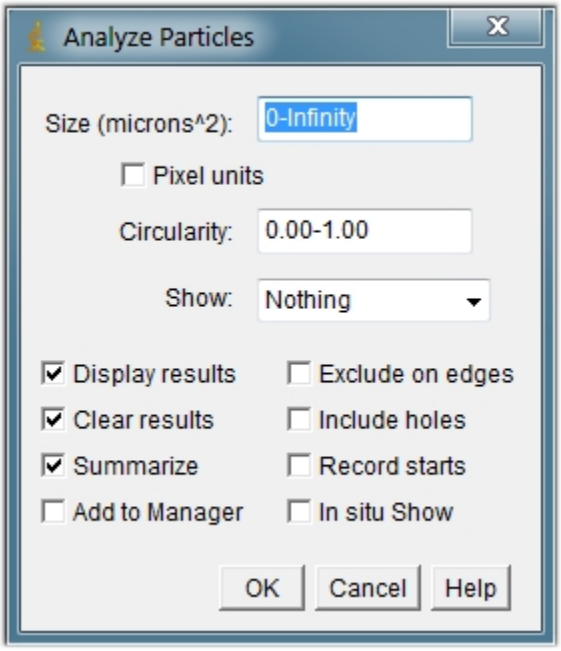

12. Two new windows open with the results and summary, which the default setting is to save as a Microsoft Excel file.

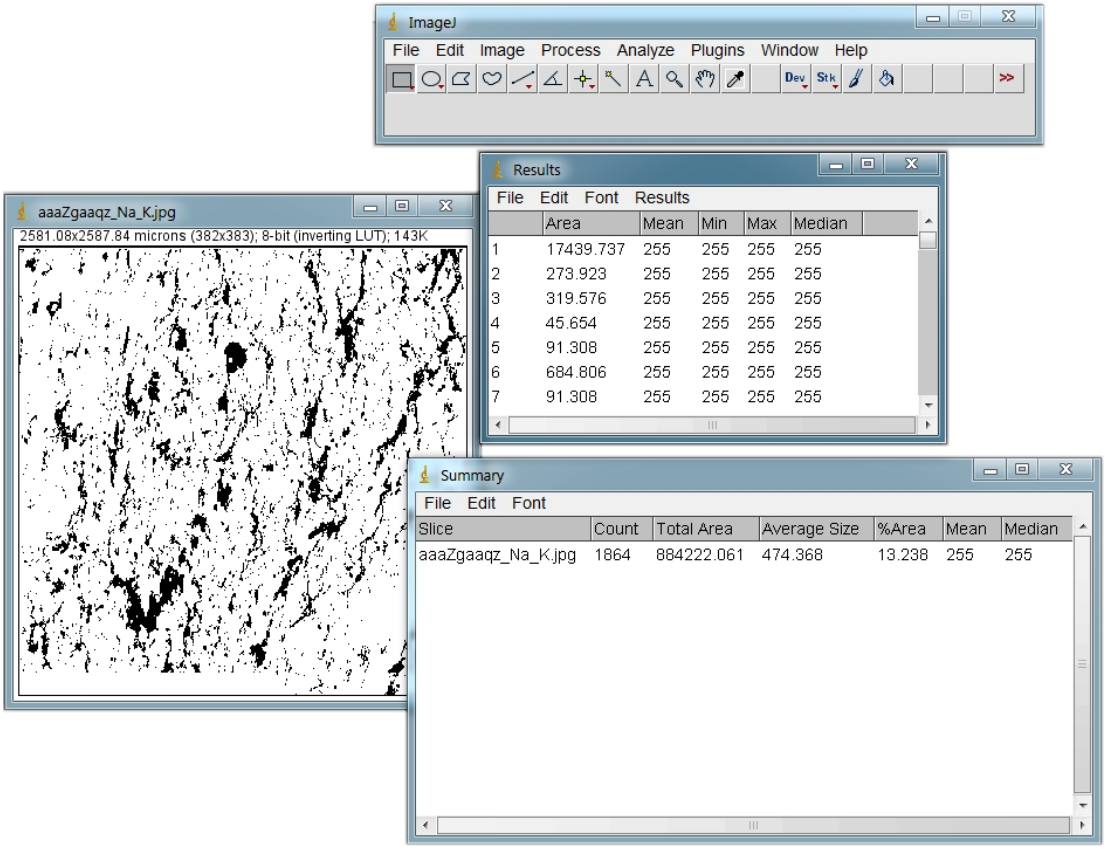

Choose to Save As or Open from the File tab. If adding more data, minimize the Summary window and start from step 1. The following results will be placed underneath the former results.

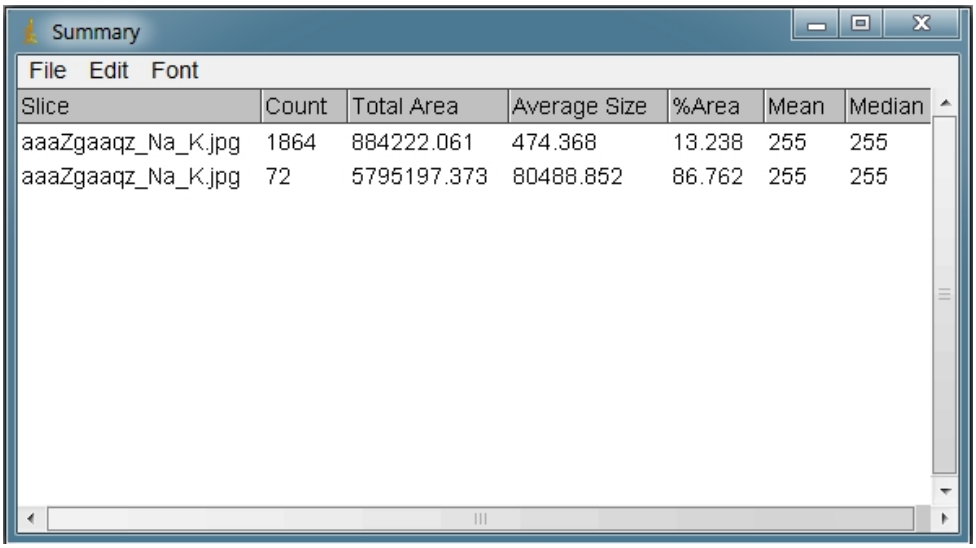

Appendix C

Table C1

Spectrometer Configuration, the First Run, December 14, 2013

Counter/ Crystal	Ch 1) PETJ + TAP		Ch 2) PETJ + GF		Ch 3) TAPH		Ch 4) TAP		Ch 5) LIFH	
Calibration/ Standard	K 120.204 mm	Kα on KK STD	Cr 72.640 mm	Kα on Chromite	Na 129.573 mm	Kα on Albite	Si 77.269 mm	Kα on Olivine	Mn 146.350 mm	Kα on MnO
	Ca 108.034 mm	Kα on Apatite STD	Ti 87.469 mm	Kα on Titanite	Mg 107.565 mm	Kα on Olivine	Al 90.470 mm	Kα on YAG	Fe 134.856 mm	Kα on Margarite
			Ba 88.301 mm	Lα on Barite			Sr 74.427 mm	Lα on Celestine	Eu 147.670 mm	Lα on Drake REE1

Spectrometer Configuration, the Second Run, December 15, 2013

Counter/ Crystal	Ch 1) PETJ + TAP		Ch 2) PETJ + GF		Ch 3) TAPH		Ch 4) TAP		Ch 5) LIFH	
Calibration/ Standard	K 120.174 mm	Kα on KK STD	Cr 72.699 mm	Kα on Chromite	Na 129.542 mm	Kα on Albite	Si 77.263 mm	Kα on Olivine	Mn 146.398 mm	Kα on MnO
	Ca 108.019 mm	Kα on Apatite STD	Ti 87.461 mm	Kα on Titanite	Mg 107.513 mm	Kα on Olivine	Al 90.475 mm	Kα on YAG	Fe 134.860 mm	Kα on Margarite
			Ba 88.281 mm	Lα on Barite			Sr 74.424 mm	Lα on Celestine	Eu 147.715 mm	Lα on Drake REE1

Spectrometer Configuration, the Third Run, December 16, 2013

Counter/ Crystal	Ch 1) PETJ + TAP		Ch 2) PETJ + GF		Ch 3) TAPH		Ch 4) TAP		Ch 5) LIFH	
Calibration/ Standard	K 120.136 mm	Kα on KK STD	Cr 72.671 mm	Kα on Chromite	Na 129.543 mm	Kα on Albite	Si 77.264 mm	Kα on Olivine	Mn 146.152 mm	Kα on MnO
	Ca 108.075 mm	Kα on Apatite STD	Ti 87.431 mm	Kα on Titanite	Mg 107.560 mm	Kα on Olivine	Al 90.469 mm	Kα on YAG	Fe 134.858 mm	Kα on Margarite
			Ba 88.308 mm	Lα on Barite			Sr 74.429 mm	Lα on Celestine	Eu 147.668 mm	Lα on Drake REE1

Table C2 - Peggy's Cove

Orthoclase	1	2	3	4	5	6	7	8	9
SiO2	61.894	62.358	62.411	62.091	61.998	61.746	62.157	62.672	61.940
TiO2	0.024	0.000	0.029	0.056	0.003	0.023	0.028	0.006	0.045
Al2O3	17.291	17.156	17.175	17.301	16.949	16.901	17.157	17.488	17.235
FeO	0.052	0.045	0.042	0.041	0.007	0.026	0.021	0.052	0.039
MnO	0.033	0.000	0.035	0.021	0.034	0.018	0.034	0.011	0.024
MgO	0.000	0.000	0.000	0.000	0.000	0.000	0.000	0.000	0.000
CaO	0.034	0.063	0.024	0.052	0.110	0.021	0.015	0.055	0.015
Na2O	0.747	1.399	0.964	1.116	0.561	0.415	1.006	1.052	0.778
K2O	14.811	13.996	14.786	14.347	15.160	15.170	14.715	14.903	15.164
BaO	0.415	0.339	0.274	1.091	0.210	0.292	0.270	0.305	0.357
SrO	0.501	0.487	0.451	0.450	0.489	0.481	0.493	0.521	0.514
Eu2O3	0.021	0.000	0.032	0.029	0.070	0.000	0.056	0.035	0.004
Cr2O3	0.000	0.000	0.000	0.000	0.000	0.000	0.000	0.000	0.000
Total	95.823	95.843	96.223	96.595	95.591	95.093	95.952	97.100	96.115
Si	2.998	3.008	3.006	2.994	3.011	3.013	3.004	2.996	2.997
Ti	0.001	0.000	0.001	0.002	0.000	0.001	0.001	0.000	0.002
Al	0.987	0.975	0.975	0.983	0.970	0.972	0.977	0.985	0.983
Fe	0.002	0.002	0.002	0.002	0.000	0.001	0.001	0.002	0.002
Mn	0.001	0.000	0.001	0.001	0.001	0.001	0.001	0.000	0.001
Mg	0.000	0.000	0.000	0.000	0.000	0.000	0.000	0.000	0.000
Ca	0.002	0.003	0.001	0.003	0.006	0.001	0.001	0.003	0.001
Na	0.070	0.131	0.090	0.104	0.053	0.039	0.094	0.098	0.073
K	0.915	0.861	0.909	0.883	0.939	0.944	0.907	0.909	0.936
Ba	0.008	0.006	0.005	0.021	0.004	0.006	0.005	0.006	0.007
Sr	0.014	0.014	0.013	0.013	0.014	0.014	0.014	0.014	0.014
Eu	0.000	0.000	0.001	0.000	0.001	0.000	0.001	0.001	0.000
Cr	0.000	0.000	0.000	0.000	0.000	0.000	0.000	0.000	0.000
Totals	5.000	5.000	5.004	5.005	4.999	4.992	5.007	5.014	5.015
Mole % of End-members									
Albite (AB, Na)	7.104	13.143	9.002	10.546	5.298	3.987	9.409	9.665	7.228
Anorthite AN, Ca)	0.179	0.327	0.124	0.271	0.574	0.111	0.077	0.279	0.077
Orthoclase (OR, K)	92.717	86.530	90.874	89.182	94.128	95.902	90.514	90.056	92.695

Perthite	1	2	3
SiO2	62.579	63.024	64.129
TiO2	0.018	0.000	0.000
Al2O3	18.397	18.413	17.087
FeO	0.038	0.027	0.000
MnO	0.000	0.023	0.023
MgO	0.000	0.000	0.000
CaO	2.407	1.690	0.211
Na2O	10.862	10.058	11.949
K2O	0.110	0.226	0.182
BaO	0.010	0.001	0.000
SrO	0.386	0.396	0.394
Eu2O3	0.000	0.003	0.000
Cr2O3	0.000	0.000	0.000
Total	94.807	93.861	93.975
Si	2.925	2.956	3.007
Ti	0.001	0.000	0.000
Al	1.013	1.018	0.944
Fe	0.001	0.001	0.000
Mn	0.000	0.001	0.001
Mg	0.000	0.000	0.000
Ca	0.121	0.085	0.011
Na	0.984	0.915	1.086
K	0.007	0.014	0.011
Ba	0.000	0.000	0.000
Sr	0.010	0.011	0.011
Eu	0.000	0.000	0.000
Cr	0.000	0.000	0.000
Totals	5.063	4.999	5.070
Mole % of End-members			
Albite (AB, Na)	88.565	90.283	98.061
Anorthite AN, Ca)	10.845	8.383	0.957
Orthoclase (OR, K)	0.590	1.335	0.983

Plagioclase Inclusion	1	2	3	4	5
SiO2	58.424	57.413	57.519	60.591	59.927
TiO2	0.000	0.003	0.024	0.019	0.008
Al2O3	21.543	21.842	21.937	20.672	20.104
FeO	0.154	0.032	0.028	0.005	0.018
MnO	0.000	0.024	0.035	0.015	0.000
MgO	0.000	0.000	0.000	0.000	0.000
CaO	5.689	8.789	8.891	5.665	5.481
Na2O	8.207	8.035	8.194	9.498	9.629
K2O	1.266	0.276	0.309	0.186	0.254
BaO	0.058	0.097	0.141	0.089	0.000
SrO	0.394	0.363	0.384	0.409	0.368
Eu2O3	0.004	0.007	0.000	0.001	0.000
Cr2O3	0.000	0.000	0.000	0.000	0.000
Total	95.739	96.881	97.462	97.150	95.789
Si	2.747	2.684	2.678	2.795	2.804
Ti	0.000	0.000	0.001	0.001	0.000
Al	1.194	1.203	1.204	1.124	1.108
Fe	0.006	0.001	0.001	0.000	0.001
Mn	0.000	0.001	0.001	0.001	0.000
Mg	0.000	0.000	0.000	0.000	0.000
Ca	0.287	0.440	0.443	0.280	0.275
Na	0.748	0.728	0.740	0.849	0.873
K	0.076	0.016	0.018	0.011	0.015
Ba	0.001	0.002	0.003	0.002	0.000
Sr	0.011	0.010	0.010	0.011	0.010
Eu	0.000	0.000	0.000	0.000	0.000
Cr	0.000	0.000	0.000	0.000	0.000
Totals	5.069	5.087	5.099	5.073	5.086
Mole % of End-members	1.000	2.000	3.000	4.000	5.000
Albite (AB, Na)	67.361	61.462	61.560	74.489	75.082
Anorthite AN, Ca)	25.802	37.149	36.912	24.551	23.615
Orthoclase (OR, K)	6.837	1.389	1.527	0.960	1.303

Table C3 - Prospect

Orthoclase	1	2	3	4	5	6	7	8
SiO2	63.993	64.304	63.551	63.156	63.063	62.745	62.671	62.739
TiO2	0.057	0.038	0.030	0.022	0.001	0.056	0.047	0.033
Al2O3	18.232	18.105	17.713	17.606	17.837	17.270	17.417	17.329
FeO	0.093	0.051	0.053	0.029	0.043	0.032	0.044	0.045
MnO	0.007	0.000	0.016	0.009	0.025	0.000	0.004	0.012
MgO	0.000	0.000	0.000	0.000	0.000	0.000	0.000	0.000
CaO	0.102	0.081	0.062	0.054	0.067	0.045	0.042	0.037
Na2O	0.890	0.780	1.359	1.239	1.112	1.556	1.472	1.310
K2O	11.723	11.664	12.391	13.398	13.043	13.663	13.467	13.925
BaO	0.549	0.411	0.337	0.284	0.441	0.472	0.741	0.551
SrO	0.451	0.403	0.416	0.399	0.453	0.423	0.411	0.406
Eu2O3	0.031	0.000	0.010	0.006	0.021	0.036	0.026	0.035
Cr2O3	0.000	0.000	0.000	0.000	0.000	0.000	0.000	0.000
Total	96.128	95.837	95.938	96.202	96.106	96.298	96.342	96.422
Si	3.023	3.037	3.023	3.014	3.010	3.008	3.005	3.008
Ti	0.002	0.001	0.001	0.001	0.000	0.002	0.002	0.001
Al	1.015	1.008	0.993	0.990	1.003	0.976	0.984	0.979
Fe	0.004	0.002	0.002	0.001	0.002	0.001	0.002	0.002
Mn	0.000	0.000	0.001	0.000	0.001	0.000	0.000	0.000
Mg	0.000	0.000	0.000	0.000	0.000	0.000	0.000	0.000
Ca	0.005	0.004	0.003	0.003	0.003	0.002	0.002	0.002
Na	0.082	0.071	0.125	0.115	0.103	0.145	0.137	0.122
K	0.707	0.703	0.752	0.816	0.794	0.836	0.824	0.852
Ba	0.010	0.008	0.006	0.005	0.008	0.009	0.014	0.010
Sr	0.012	0.011	0.011	0.011	0.013	0.012	0.011	0.011
Eu	0.001	0.000	0.000	0.000	0.000	0.001	0.000	0.001
Cr	0.000	0.000	0.000	0.000	0.000	0.000	0.000	0.000
Totals	4.861	4.845	4.918	4.956	4.937	4.992	4.981	4.988
Mole % of End-members	1.000	2.000	3.000	4.000	5.000	6.000	7.000	8.000
Albite (AB, Na)	10.283	9.177	14.234	12.291	11.424	14.719	14.214	12.486
Anorthite AN, Ca)	0.651	0.527	0.359	0.296	0.380	0.235	0.224	0.195
Orthoclase (OR, K)	89.066	90.297	85.407	87.413	88.195	85.046	85.562	87.319

Coarse Perthite	1	2	3	4	5	6
SiO2	69.665	66.582	52.650	66.507	66.925	66.067
TiO2	0.002	0.000	0.038	0.000	0.018	0.001
Al2O3	19.221	19.113	31.142	19.767	20.558	19.766
FeO	0.048	0.023	0.106	0.037	0.039	0.029
MnO	0.004	0.000	0.009	0.000	0.000	0.020
MgO	0.000	0.000	0.000	0.000	0.000	0.000
CaO	0.453	1.365	0.190	2.321	1.543	2.295
Na2O	3.229	6.660	3.069	5.548	3.879	5.258
K2O	0.077	0.137	6.285	0.148	0.606	0.132
BaO	0.009	0.006	0.171	0.066	0.059	0.000
SrO	0.395	0.391	0.279	0.375	0.430	0.389
Eu2O3	0.000	0.000	0.010	0.014	0.000	0.000
Cr2O3	0.000	0.000	0.000	0.000	0.000	0.000
Total	93.103	94.277	93.949	94.783	94.057	93.957
Si	3.144	3.040	2.508	3.020	3.036	3.020
Ti	0.000	0.000	0.001	0.000	0.001	0.000
Al	1.022	1.029	1.748	1.058	1.099	1.065
Fe	0.002	0.001	0.004	0.001	0.001	0.001
Mn	0.000	0.000	0.000	0.000	0.000	0.001
Mg	0.000	0.000	0.000	0.000	0.000	0.000
Ca	0.022	0.067	0.010	0.113	0.075	0.112
Na	0.283	0.590	0.283	0.488	0.341	0.466
K	0.004	0.008	0.382	0.009	0.035	0.008
Ba	0.000	0.000	0.003	0.001	0.001	0.000
Sr	0.010	0.010	0.008	0.010	0.011	0.010
Eu	0.000	0.000	0.000	0.000	0.000	0.000
Cr	0.000	0.000	0.000	0.000	0.000	0.000
Totals	4.488	4.744	4.949	4.700	4.601	4.684
Mole % of End-members	1.000	2.000	3.000	4.000	5.000	6.000
Albite (AB, Na)	91.473	88.748	41.989	80.082	75.609	79.511
Anorthite AN, Ca)	7.091	10.051	1.436	18.512	16.619	19.176
Orthoclase (OR, K)	1.435	1.201	56.575	1.406	7.772	1.313

Fine Perthite	1	2	3	4	5	6
SiO2	67.000	67.544	67.140	64.097	64.270	64.407
TiO2	0.000	0.000	0.000	0.002	0.013	0.017
Al2O3	18.961	18.703	18.382	17.658	17.566	17.280
FeO	0.016	0.030	0.024	0.022	0.030	0.020
MnO	0.000	0.000	0.002	0.003	0.000	0.000
MgO	0.000	0.000	0.000	0.000	0.000	0.000
CaO	1.026	0.462	0.299	0.249	0.752	0.354
Na2O	5.503	6.221	6.915	11.220	11.660	13.262
K2O	0.286	0.167	0.226	0.231	0.212	0.154
BaO	0.000	0.025	0.003	0.052	0.028	0.000
SrO	0.401	0.357	0.411	0.381	0.324	0.348
Eu2O3	0.000	0.000	0.000	0.000	0.000	0.000
Cr2O3	0.000	0.000	0.000	0.000	0.000	0.000
Total	93.193	93.509	93.402	93.915	94.855	95.842
Si	3.074	3.087	3.083	2.999	2.988	2.979
Ti	0.000	0.000	0.000	0.000	0.000	0.001
Al	1.025	1.008	0.995	0.974	0.962	0.942
Fe	0.001	0.001	0.001	0.001	0.001	0.001
Mn	0.000	0.000	0.000	0.000	0.000	0.000
Mg	0.000	0.000	0.000	0.000	0.000	0.000
Ca	0.050	0.023	0.015	0.012	0.037	0.018
Na	0.489	0.551	0.616	1.018	1.051	1.190
K	0.017	0.010	0.013	0.014	0.013	0.009
Ba	0.000	0.000	0.000	0.001	0.001	0.000
Sr	0.011	0.009	0.011	0.010	0.009	0.009
Eu	0.000	0.000	0.000	0.000	0.000	0.000
Cr	0.000	0.000	0.000	0.000	0.000	0.000
Totals	4.667	4.690	4.734	5.030	5.062	5.148
Mole % of End-members	1.000	2.000	3.000	4.000	5.000	6.000
Albite (AB, Na)	87.933	94.456	95.658	97.484	95.456	97.810
Anorthite AN, Ca)	9.060	3.876	2.285	1.195	3.402	1.443
Orthoclase (OR, K)	3.007	1.668	2.057	1.321	1.142	0.747

Plagioclase Inclusion	1	2	3	4	5	6
SiO2	64.385	65.914	64.465	65.481	66.982	60.122
TiO2	0.000	0.001	0.000	0.005	0.031	0.041
Al2O3	19.746	19.796	18.700	18.574	18.427	16.880
FeO	0.028	0.026	0.009	0.026	0.031	0.049
MnO	0.000	0.000	0.000	0.000	0.000	0.015
MgO	0.000	0.000	0.000	0.000	0.000	0.000
CaO	2.909	2.324	1.554	1.043	0.247	0.031
Na2O	7.123	5.454	8.597	8.106	7.139	1.158
K2O	0.171	0.139	0.247	0.211	0.233	11.422
BaO	0.028	0.000	0.000	0.078	0.000	0.851
SrO	0.382	0.342	0.366	0.351	0.394	0.366
Eu2O3	0.000	0.012	0.000	0.000	0.000	0.014
Cr2O3	0.000	0.000	0.000	0.000	0.000	0.000
Total	94.392	93.717	93.479	93.442	93.103	90.887
Si	2.959	3.015	2.992	3.025	3.077	3.021
Ti	0.000	0.000	0.000	0.000	0.001	0.002
Al	1.070	1.067	1.023	1.011	0.997	1.000
Fe	0.001	0.001	0.000	0.001	0.001	0.002
Mn	0.000	0.000	0.000	0.000	0.000	0.001
Mg	0.000	0.000	0.000	0.000	0.000	0.000
Ca	0.143	0.114	0.077	0.052	0.012	0.002
Na	0.635	0.484	0.774	0.726	0.636	0.113
K	0.010	0.008	0.015	0.012	0.014	0.732
Ba	0.001	0.000	0.000	0.001	0.000	0.017
Sr	0.010	0.009	0.010	0.009	0.010	0.011
Eu	0.000	0.000	0.000	0.000	0.000	0.000
Cr	0.000	0.000	0.000	0.000	0.000	0.000
Totals	4.828	4.698	4.891	4.838	4.748	4.900
Mole % of End-members	1.000	2.000	3.000	4.000	5.000	6.000
Albite (AB, Na)	80.551	79.858	89.383	91.893	96.099	13.321
Anorthite AN, Ca)	18.177	18.803	8.928	6.533	1.837	0.197
Orthoclase (OR, K)	1.272	1.339	1.690	1.574	2.064	86.482

Appendix D

Electronic Data Supplement: Electron Microprobe Point Data and Line Scan Data

Appendix E

Mechanical Issues and Changes

The start point of Map 1 was set to the coordinates 32.3412, 49.1566, the margin of the megacryst. A reset of the system was necessary to correct for SiO_2 inconsistencies; additionally, the removal of Mg and Cr from element menu to create vacancies for Sr and Eu. Although, these issues occurred, the results have been corrected to ensure the data had little chance of error.